Water Resources Research

RESEARCH ARTICLE
10.1029/2019WR025813

Special Section:
Advances in remote sensing, measurement, and simulation of seasonal snow

The Value of Long-Term (40 years) Airborne Gamma Radiation SWE Record for Evaluating Three Observation-Based Gridded SWE Data Sets by Seasonal Snow and Land Cover Classifications

Eunsang Cho[1,2], Jennifer M. Jacobs[1,2], and Carrie M. Vuyovich[3]

[1]Department of Civil and Environmental Engineering, University of New Hampshire, Durham, NH, USA, [2]Earth Systems Research Center, Institute for the Study of Earth, Oceans, and Space, University of New Hampshire, Durham, NH, USA, [3]Hydrological Sciences Laboratory, NASA Goddard Space Flight Center, Greenbelt, MD, USA

Key Points:
- Long-term airborne gamma radiation observations provide reliable SWE observations even over forest regions
- University of Arizona (UA) SWE has the strongest agreement with gamma SWE regardless of seasonal snow and land cover class
- Large differences occur when the tree cover is 80% or higher, the slope is steeper than 2.5°, and the elevation range exceeds 100 m

Supporting Information:
- Supporting Information

Correspondence to:
E. Cho,
ec1072@wildcats.unh.edu

Citation:
Cho, E., Jacobs, J. M., & Vuyovich, C. M. (2020). The value of long-term (40 years) airborne gamma radiation SWE record for evaluating three observation-based gridded SWE data sets by seasonal snow and land cover classifications. *Water Resources Research*, *56*, e2019WR025813. https://doi.org/10.1029/2019WR025813

Received 1 JUL 2019
Accepted 18 DEC 2019
Accepted article online 21 DEC 2019

Abstract Observation-based long-term gridded snow water equivalent (SWE) products are important assets for hydrological and climate research. However, an evaluation of the currently available SWE products has been limited due to the lack of independent SWE data that extend over a large range of environmental conditions. In this study, three daily long-term SWE products (Special Sensor Microwave Imager and Sounder [SSMI/S] SWE, GlobSnow-2 SWE, and University of Arizona [UA] SWE) were evaluated by seasonal snow cover and land cover classifications over the conterminous United States from 1982 to 2017, using the historical airborne gamma radiation SWE observations (20,738 measurements). We found that there are similar patterns in SSMI/S and GlobSnow-2 SWE when compared against the gamma SWE. However, GlobSnow-2 SWE had better agreement with gamma SWE than SSMI/S SWE in some forested-type classes and maritime and prairie snow classes. As compared to SSMI/S and GlobSnow-2 SWE, UA SWE has much better agreement with gamma SWE in all land cover types and snow classes. Tree cover and topographic heterogeneity affect the agreement between the gamma and gridded SWE and accuracy of gamma SWE itself with the largest differences typically occurring when the percent tree cover was 80% or higher, the terrain slope was steeper than 2.5°, and the elevation range exceeded 100 m. The results demonstrate the reliability of the UA SWE products and the benefits of the gamma radiation approach to measure SWE, especially in forested regions.

Plain Language Summary Long-term gridded snowpack data are essential for effective water resource management and flood risk assessments under a changing climate in the United States. However, the currently available snowpack data have large uncertainties, and the evaluations have been limited due to the lack of reliable independent data sets. Here, we evaluate three daily long-term (>30 years) snow water equivalent (SWE) products—empirically based SWE from passive microwave, GlobSnow-2 SWE, and University of Arizona SWE from 1982 to 2017 over the conterminous United States—using the historical airborne gamma SWE observations collected by the National Oceanic and Atmospheric Administration. Two key findings are that (1) the UA SWE product is the most reliable and (2) the long-term airborne SWE record is of great value, especially in forested regions.

1. Introduction

Snow impacts human activity across the United States as a source of water, hydropower, and potentially flooding. In the western United States, snow supplies 70% of the annual water supply valued at more than $348 billion per year (Adams et al., 2004). In the north-central and northeastern United States, snow meltwater is a dominant driver of severe spring flooding (Wazney & Clark, 2015; Stadnyk et al., 2016; https://www.weather.gov/dvn/summary_SpringFlooding_2019). Accurate, timely estimates of the snowpack are required over the United States to help monitor and manage seasonal snow and melt. The most hydrologically relevant measure of the snowpack is snow water equivalent (SWE), which describes the amount of water stored in the snow.

In addition to real-time snow observations, a long-term record of SWE is important for identifying climate variability and trends and for developing a climatology of the snowpack. As changes in seasonal snow

have recently accelerated across the United States in the last few decades (Ashfaq et al., 2013; Georgakakos et al., 2014), reliable long-term SWE measurements are further needed for effective water management and flood risk assessments (Zeng et al., 2018). Point-based long-term SWE records from snow station networks (e.g., NRCS Snowpack Telemetry [SNOTEL]) have provided high-quality measurements. The time series of SWE observations have been used to evaluate and validate trends and seasonal variabilities in snowpack in numerous previous studies in the western United States (Cooper et al., 2016; Mote et al., 2018; Pierce et al., 2008). However, point measurements do not necessarily represent the snowpack distribution especially in areas with spatially heterogeneous terrain (Molotch & Bales, 2005). In order to overcome the limitations, observation-based gridded SWE products have been developed using satellite remote sensing and/or in situ snow station networks with assimilation techniques.

A series of passive microwave satellite sensors have provided a potential source of spatially distributed SWE information. For more than 30 years, the Special Sensor Microwave Imager (SSM/I) and SSM Imager/Sounder (SSMIS) aboard the Defense Meteorological Satellite Program (DMSP) series of satellites (1987—current) have provided long-term SWE information at a global scale (Derksen et al., 2005; Foster et al., 2005; Tait, 1998). Passive microwave SWE retrieval algorithms typically use empirical relationships between SWE and snow depth and the difference between the brightness temperatures at two different passive microwave frequencies: a low frequency, 18–19 GHz, and a higher frequency, typically around 37 GHz. However, known sources of error hamper the operational use in many regions over the United States. Carroll et al. (1999) mentioned major difficulties that tend to be inherent in the satellite-based passive microwave SWE products. First, the passive microwavse algorithms tend not to work under a deep snowpack (greater than approximately 200-mm SWE), which is called "saturation effect" because the higher frequency microwave signal is no longer detectable (Dong et al., 2005; Vuyovich et al., 2017). Second, the general tendency is for algorithms to not estimate SWE sufficiently well in forested or heavily vegetated regions (Foster et al., 2005; Vander Jagt et al., 2013). Third, even in flat areas with sparse vegetation, the passive microwave signal is highly sensitive to even small amounts of liquid water in the snowpack (Kang et al., 2014; Walker & Goodison, 1993). Consequently, the SWE values are unreliable under wet snow conditions.

To directly assimilate satellite-based passive microwave emission, Pulliainen (2006) developed a Bayesian-based assimilation technique that weighs the passive microwave satellite data and the interpolated ground-based snow depth observations using a semi-empirical radiative transfer model. This assimilation technique was integrated into the GlobSnow project supported by the European Space Agency to produce a long-term SWE data set for the Northern Hemisphere (Takala et al., 2011). Because ground-based snow depth was used to generate interpolated effective grain size data and simulate Tb and SWE, the accuracy of the SWE is expected to be better than those of typical stand-alone channel differencing algorithms from passive microwave satellite sensors (e.g., Chang et al., 1987; Kelly, 2009). In fact, previous studies found that the GlobSnow SWE has better performance with point ground SWE measurements as compared to the empirical SWE algorithms (Hancock et al., 2013; Larue et al., 2017; Mudryk et al., 2015). However, the GlobSnow-2 SWE still has large uncertainties with root-mean-square error (RMSE) of 94 mm (36%) in wet and deep snow conditions and forested regions, probably due to the inherent sources of error in passive microwave signal (Larue et al., 2017). Hancock et al. (2013) using GlobSnow V1.0 also reported that occasional abrupt changes were found in the product.

The University of Arizona (UA) recently developed a 4-km gridded long-term SWE data set from 1982 to 2017 (hereafter UA SWE) over the conterminous United States (Broxton et al., 2016) by combining high-quality point SWE measurements with finer spatial resolution gridded precipitation and temperature data sets. The observation-based UA SWE product is produced by interpolating thousands of ground-based measurements of SWE and snow depth from SNOTEL (Serreze et al., 1999) and the NWS Cooperative Observer Program (COOP) network sites and 4-km gridded PRISM precipitation and temperature data (Daly et al., 2008). The quality and reliability of the UA SWE data have been demonstrated compared to reanalysis and land assimilation products (Broxton et al., 2016) and independent observation-based products (Dawson et al., 2018). Dawson et al. (2018) reported that the passive microwave AMSR-E SWE product and two satellite-merged SWE products (GlobSnow-2 and Canadian Sea Ice and Snow Evolution Network) have large differences from the UA SWE data (mean absolute difference [MAD]: 46% to 59%), especially in forested regions. They also found that there was a good agreement in basin-averaged SWE between UA and Airborne Snow Observatory (ASO) products (32 flight measurements) (Painter et al.,

2016) in the upper Tuolumne basin, California's Sierra Nevada (correlation: 0.98 and MAD: 51.5 mm [30%]). However, since the test with ASO SWE had a limited number of flights over a sparsely forested region (<30% of tree cover fraction; Dawson et al., 2018), there is still a need to further evaluate the accuracy of the UA SWE over more heavily vegetated regions.

Due to the lack of reliable independent SWE records, an evaluation of the currently available long-term SWE products at a continental scale has been limited. The airborne gamma snow survey operated by the National Oceanic and Atmospheric Administration's (NOAA) National Operational Hydrologic Remote Sensing Center (NOHRSC) has substantial potential to evaluate the gridded SWE products over the conterminous United States. The NOAA airborne gamma snow survey was designed to help hydrologists and flood forecasters in the National Weather Service offices, regional river forecasting centers, and other U.S. and Canadian federal agencies improve operational spring flood predictions and water supply outlooks (Peck et al., 1980). Since 1979, the snow survey has collected areal mean SWE data over a network of 2,400 flight lines covering 25 states and seven Canadian provinces (Carroll, 2001). The airborne gamma technique uses the attenuation of the gamma-ray signal by water in the snowpack (any phase) to measure SWE for each flight line. The mean areal gamma SWE value is based on the difference between gamma radiation measurements over bare ground and snow-covered ground.

The accuracy of airborne gamma SWE estimates has been evaluated using numerous ground-based snow observations from snow courses and field campaigns on designated flight lines (Carroll & Schaake, 1983; Carroll & Vose, 1984; Glynn et al., 1988; Goodison et al., 1984; Peck et al., 1971). In prairie regions, with mean ground-based SWE between 20 and 150 mm, the RMSE of airborne gamma SWE is less than 10 mm (4–10%) based on a few hundred samples within the flight lines (Carroll & Schaake, 1983). In densely forested regions, Carroll and Vose (1984) found that the airborne gamma SWE had a low bias and an RMSE of 23 mm as compared to the mean ground-based SWE. In that study of the Lake Superior and Saint John basins in the United States, SWE measurements ranged from 20 to 480 mm based on approximately 200 snow depth measurements and 20 snow density measurements distributed along the length of each flight line (total 72 lines). These studies provided the impetus to develop an airborne gamma SWE program, which has been successfully used for operational flood forecasting during the last 40 years (Carroll, 2001). Currently, the airborne gamma SWE observations, as well as ground-based and satellite snow covered area observations over the United States, support the NOHRSC near-real-time, high spatial resolution (1 km^2 gridded) Snow Data Assimilation System products (Barrett, 2003).

An evaluation of the currently available long-term SWE products is important to differentiate among environments having a strong agreement or large differences among products. The 40-year airborne gamma SWE record is ideal to evaluate the gridded observation-based SWE products according to seasonal snow and land cover characteristics. Even though the gamma SWE record has limited spatial and temporal coverages compared to the coarser satellite and assimilation products, the record provides accurate and reliable SWE in a wide range of snow and land characteristics, especially in forested regions where SWE estimation remains challenging (Cho et al., 2018). The wide range encompasses a broader sample of snow conditions over a longer time period than is collected using any other aerial observations (e.g., airborne lidar) and provides spatially integrated observations over a footprint closer to satellite resolution than point observations.

This study focuses on providing a comprehensive examination of three currently available observation-based gridded SWE data sets, spaceborne passive microwave SSM/I-SSMIS (hereafter SSMI/S) SWE, GlobSnow-2 SWE, and UA SWE, using the airborne gamma SWE record from 1982 to 2017 over the conterminous United States. We hypothesize that SSMI/S, using a standard Chang-type microwave retrieval algorithm, and GlobSnow-2 products will show similar patterns as compared to the airborne gamma SWE estimates, that is, good agreement in regions with little vegetation and relatively homogeneous terrain (e.g., cropland and grassland land cover types and "prairie" of seasonal snow class) and lower agreement in regions with dense vegetation and heterogeneous terrain (e.g., forested-type land cover types and "warm forest" and "maritime" of seasonal snow classes). We also hypothesize that UA SWE will compare favorably to the gamma SWE even in forested or heavily vegetated regions due to the lower impact of forest fraction on both products (Cho et al., 2018; Dawson et al., 2018). Finally, we hypothesize that known gamma weaknesses under heterogeneous conditions will be revealed as larger differences between gamma SWE and the gridded

products. We evaluate the three long-term daily SWE estimates against the historical airborne gamma SWE record by land cover type, seasonal snow cover classification, and the degree of the tree fraction and land heterogeneity across the United States.

This paper is organized as follows. Section 2 describes the study area with land cover types, seasonal snow classes, and tree fractions for a categorized evaluation and sensitivity test of the SWE products. Section 3 describes the three gridded SWE data sets and airborne gamma SWE. The methodologies, which include a resampling method and the calculation of agreement statistics, are described in section 4. Section 5 details the results of spatial comparison of three products (section 5.1), their differences by seasonal snow and land cover classes (section 5.2), and the effect of tree fraction and topographical characteristics (section 5.3). Section 6 offers discussions about the similarities, differences, and new findings in our results with respect to previous studies and potential limitations of gamma SWE estimates. Conclusion and future perspectives are drawn in section 7.

2. Study Area

The study area comprises the conterminous United States where all SWE data used in this study are available (Figure 1), including parts of eight NOAA river forecasting centers (RFCs): North-Central (NC), Missouri Basin (MB), Ohio (OH), North-East (NE), Mid-Atlantic (MA), Colorado Basin RFC (CB), Northwest (NW), and California Nevada (CN). The RFC boundaries were designated by the NOAA NWS Advanced Hydrological Prediction Service to manage regional river flow and support flood forecasting over the United States. The airborne gamma radiation survey provides fall soil moisture and winter SWE measurements to each regional RFC. The NOAA NOHRSC gamma radiation survey network is composed of over 2,400 flight lines over the United States including Alaska and southern Canada. Among them, 1,812 gamma flight lines over the conterminous United States were used in this study. The study region is dominated by seven types of the International Geosphere-Biosphere Programme (IGBP) land cover type: evergreen needleleaf forest, deciduous broadleaf forest, mixed forest, croplands, cropland/natural vegetation mosaic, grasslands, and woody savannas (Channan et al., 2014; Figure 1a). The study area is also classified by six seasonal snow classes: tundra, taiga, maritime, ephemeral, prairie, and warm forest by the Sturm et al. (2010) seasonal snow cover classification (Figure 1b). Due to a very limited number of gamma SWE observations, the woody savannas land cover type and the ephemeral snow classes were excluded in this study. The annual vegetation continuous field (VCF) from the NASA Making Earth System Data Records for Use in Research Environments (MEaSUREs) was used to estimate fractional tree cover at each gamma line (Hansen & Song, 2018; Figure 1c).

3. Data

3.1. Airborne Gamma Radiation SWE

The airborne SWE estimates are obtained using a gamma radiation detector onboard a low-flying aircraft (at an altitude of 150 m above the ground). This instrument measures the natural terrestrial gamma radiation emitted from trace elements of ^{40}K, ^{238}U, and ^{232}Th radioisotopes in the upper 20 cm of soil. In the airborne gamma technique, the attenuation of the gamma-ray signal by water mass in the snowpack (any phase) over a flight line is used to estimate SWE directly. The airborne gamma SWE value is estimated using the difference between the rates of gamma radiation particles over bare ground (attenuation by soil moisture only) and snow-covered ground (attenuation by soil moisture and snowpack).

The operational gamma SWE data are calculated using the following equations:

$$SWE\left(^{40}K\right) = \frac{25.4}{A}\cdot\left[ln\left[\frac{^{40}K_b}{^{40}K_s}\right] - ln\left[\frac{100 + 1.11\cdot SM\left[^{40}K_s\right]}{100 + 111\cdot SM\left[^{40}K_b\right]}\right]\right] \quad (1)$$

$$SWE\left(^{208}TI\right) = \frac{1}{A}\cdot\left[ln\left[\frac{^{208}Tl_b}{^{208}Tl_s}\right] - ln\left[\frac{100 + 1.11\cdot SM\left[^{208}Tl_s\right]}{100 + 111\cdot SM\left[^{208}Tl_b\right]}\right]\right] \quad (2)$$

$$SWE(GC) = \frac{1}{A}\cdot\left[ln\left[\frac{GC_b}{GC_s}\right] - ln\left[\frac{100 + 1.11\cdot SM[GC_s]}{100 + 111\cdot SM[GC_b]}\right]\right] \quad (3)$$

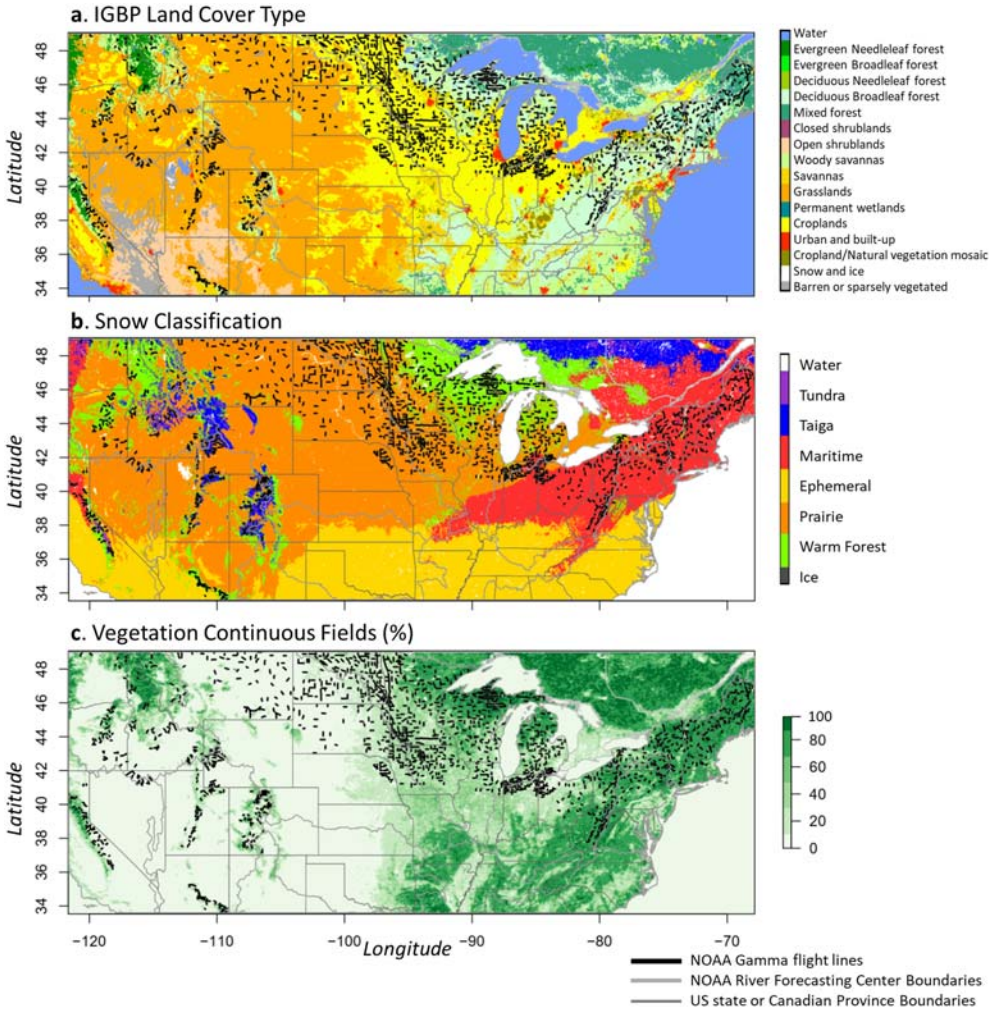

Figure 1. (a) IGBP land cover type, (b) the Sturm et al. seasonal snow classification, and (c) Vegetation Continuous Field maps of the study area over the conterminous United States with NOAA gamma flight lines ($N = 1{,}812$).

$$GammaSWE = 0.346 \cdot SWE\left({}^{40}K\right) + 0.518 \cdot SWE\left({}^{208}Tl\right) + 0.136 \cdot SWE(GC) \quad (4)$$

where ${}^{40}K$, ${}^{208}Tl$, and the total count windows (GC) are uncollided gamma count rates over bare ground (${}^{40}K_b$, ${}^{208}Tl_b$, and GC_b) and snow-covered ground (${}^{40}K_s$, ${}^{208}Tl_s$, and GC_s). SM(${}^{40}K_b$), SM(${}^{208}Tl_b$), and SM(GC_b) are gravimetric soil moisture contents over bare ground, and SM(${}^{40}K_s$), SM(${}^{208}Tl_s$), and SM(GC_s) are gravimetric soil moisture contents over snow-cover ground detected by ${}^{40}K$, ${}^{208}Tl$, and the total count windows (GC), respectively. A is a radiation attenuation coefficient in water, 0.1482. *GammaSWE* is a single average gamma radiation SWE (mm) value for the entire flight line reported via the NOHRSC website (http://www.nohrsc.noaa.gov/snowsurvey/).

Since 1979, the operational NWS gamma radiation snow survey has provided about 27,000 gamma SWE measurements over the entire U.S. and southern Canadian provinces via the NOHRSC website (http://www.nohrsc.noaa.gov/snowsurvey/). A typical flight line covers approximately 5 km^2 with a swath 300 m wide and 16 km long. The gamma SWE observations are areal-average values for each flight line footprint. In this study, 20,738 airborne gamma SWE observations covering 1,812 flight lines flown from January 1982 to May 2017 within the conterminous United States are used (Table 1). Flight lines in which the majority type/class does not exceed 50% of the gamma footprint were considered "unclassified" and were excluded from each analysis by the land cover type and snow classification.

Table 1
Overview of the Number of the NOAA Airborne Gamma Radiation Flight Lines and SWE Observations by Land Cover Types and Snow Classes

Land cover types	Flight lines	Total	1982–1989	1990–1999	2000–2009	2010–2017	Snow cover type	Flight lines	Total	1982–1989	1990–1999	2000–2009	2010–2017
Evergreen needleleaf forest	192	1,735	283	716	549	187	Tundra	99	1,346	94	631	523	98
Deciduous broadleaf forest	165	2,609	143	516	1,290	660	Taiga	72	925	62	392	391	80
Mixed forest	220	3,961	470	894	1,342	1,255	Maritime	391	5,487	485	1,299	2,365	1,338
Grasslands	368	2,640	267	1,002	1,122	249	Prairie	1,079	10,704	2,486	3,302	2,222	2,694
Croplands	610	7,140	1,931	2,174	1,038	1,997	Warm forest	69	644	159	156	157	172
Cropland/natural vegetation	245	2,582	407	873	823	479	Ephemeral	3	5	1	4	0	0
Woody savannas	12	71	48	21	0	2	Unclassified	99	1,627	262	412	506	447
Total	1,812	20,738	3,549	6,169	6,164	4,829	Total	1,812	20,738	3,549	6,169	6,164	4,829

Note. The gamma SWE values in the woody savannas, ephemeral, and unclassified are excluded in this study.

3.2. Spaceborne Passive Microwave SSM/I and SSMIS SWE

The series of SSM/I and SSMIS sensors aboard the DMSP series of satellites operated by the U.S. Department of Defense provides daily brightness temperatures at approximately 6 a.m. (descending)/p.m. (ascending) local time with global coverage from July 1987 to the present. The microwave frequencies at 19, 22, 37 (SSM/I and SSMIS), 85 (SSM/I only), and 91 GHz (SSMIS only) are sampled in both horizontal and vertical polarizations, except the 22 GHz (vertical only). In this study, SSMI/S SWE was estimated using a Chang-type algorithm (Chang et al., 1987) with original coefficients for F8–F13 (Armstrong & Brodzik, 2001) and modified coefficients for F17 developed by Brodzik (2014) as follows:

$$SWE_{SSM/I} = 4.77 \cdot \left(Tb_{H,19GHz} - Tb_{H,37GHz} - 5\right) \text{ for F8, F11, and F13 SSM/I} \quad (5)$$

$$SWE_{\text{SSMIS}} = a \cdot Tb_{H,19GHz} - b \cdot Tb_{H,37GHz} - c \text{ for F17 SSMIS} \quad (6)$$

where a, b, and c are given as 4.807 mm/K, 4.792 mm/K, and 6.036 mm, respectively. $Tb_{H,19GHz}$ and $Tb_{H,37GHz}$ are brightness temperatures at 19- and 37-GHz horizontal polarization, respectively. F8, F11, F13, and F17 are the DMSP platform ID. The Tb at the descending overpass (6 a.m.) was used to minimize error by wet snow (Derksen et al., 2000). The DMSP SSM/I-SSMIS Pathfinder Daily EASE-Grid Brightness Temperatures (Version 2) from July 1987 to May 2017 was used in this study and freely available at the National Snow and Ice Data Center (NSIDC) website (https://nsidc.org/data/NSIDC-0032; Armstrong et al., 1994).

3.3. GlobSnow-2 SWE

The GlobSnow project, funded by the European Space Agency, provides gridded daily SWE maps with 25-km spatial resolution from 1979 to 2016 (GlobSnow-2, archive_v2.0) for the Northern Hemisphere, except for glaciers and mountainous regions. The GlobSnow SWE utilizes an observation-based data assimilation approach combining ground-based synoptic snow depth station data with passive microwave satellite measurements (Takala et al., 2011). Ground-based point measurements of snow depth are taken from the European Centre for Medium-Range Weather Forecasts WMO weather stations. The final product uses daily Tb at 19 and 37 GHz in vertical polarization from the series of passive microwave radiometers (SMMR 1979–1987, SSM/I 1987–2009, and SSMIS 2010–2014) (GlobSnow-2 Final Report; Luojus et al., 2014).

The basis of the GlobSnow SWE processing system is presented by Pulliainen (2006) and Takala et al. (2011), though a brief description of the processes for SWE retrievals is given here. Snow depth maps are produced using ordinary kriging interpolation technique for synoptic weather station snow depth observations. The gridded snow depth is used as input to simulated Tb using the HUT snow emission model. The model describes Tb as a function of a single-layer snowpack (depth, snow density, and effective grain size) and forest canopy. The model is fit to satellite-observed Tb values by optimizing effective snow grain sizes with constant snow density (0.24 kg/m^2) at the locations where the weather station snow depth values are available. A map of spatially continuous effective snow grain size is developed by the weather station–based snow

grain size estimates using a kriging interpolation technique. The snow depth and effective snow grain size maps are used to initiate the HUT model as inputs and generate gridded Tb simulations. The Tb simulations are then assimilated with satellite Tb observations by using adaptive weights on the satellite-observed Tb according to their variances. A final SWE is estimated using the assimilated Tb with the maps of the effective grain size and land cover information (Takala et al., 2011).

Compared to the previous V1.0 and V1.3 SWE products, there are enhancements to the GlobSnow-2 SWE (archive_v2.0) product including the improved quantification of data uncertainty characteristics, homogenization of the multiple-year snow depth measurements from synoptic weather stations, and re-processing of the long-term SWE data sets. While the retrieval accuracy of the GlobSnow-2 SWE has remained the same for most regions, it showed slight improvements for northern boreal forest and tundra regions in Canadian reference data (Pulliainen et al., 2014). It should be noted that the inter-sensor systematic bias is not corrected in this product (Takala et al., 2011) whereas previous studies have shown inter-sensor biases in the Tb of the SMMR, SSM/I, and SSMI/S sensors (Derksen & Walker, 2003; Royer & Poirier, 2010; André et al., 2015; Cho et al., 2017). In this study, the daily GlobSnow-2 SWE was used from January 1982 to December 2016, which was obtained from http://www.globsnow.info/swe/archive_v2.0/.

3.4. UA SWE

The UA SWE is an observation-based 4-km gridded SWE data set recently developed by combining the SNOTEL SWE and NWS COOP snow depth measurements with the gridded PRISM precipitation and temperature data over the conterminous United States (Zeng et al., 2018). A new interpolation technique was used to produce the gridded SWE data set based on the ratio of observed SWE over net accumulated snowfall (accumulated snowfall minus cumulative snow ablation), rather than SWE itself (Broxton, Dawson, & Zeng, 2016). For this, daily precipitation data were divided into daily snowfall versus rainfall using a daily air temperature (2 m) threshold, and then, accumulated snow was calculated as the sum of the daily snowfalls. Daily cumulative snow ablation at each station (or grid cell) is taken from a relationship between the SNOTEL-based cumulative snow ablation and cumulative degree days above 0 °C established by the entire SNOTEL network (figure 2b in Broxton, Dawson, & Zeng, 2016). The UA SWE product also uses a newly developed snow density parameterization, which was called "SNODEN" (Dawson et al., 2017). This parameterization attempts to include physical processes (e.g., temperature-based aging, overburden snowpack, and liquid water from snowmelt) based on the SNOTEL SWE and air temperature at 2 m by seasonal snow cover classes. The parameterization was used to convert COOP snow depth data into SWE estimates and compute gridded snow depth from the gridded SWE data. In this study, the daily UA SWE is used from January 1982 to December 2017. The product is available from the NASA NSIDC website (https://nsidc.org/data/nsidc-0719).

3.5. Land Cover Type, Snow Classification, Tree Cover Fraction, and Topographic Heterogeneity

In this study, the IGBP land cover type, the Sturm et al. snow classification, and the VCF data were used to evaluate the long-term SWE estimates with the airborne gamma SWE considering land cover and snow characteristics as well as the tree cover fraction across the United States. The Terra and Aqua combined Moderate Resolution Imaging Spectroradiometer (MODIS) land cover data (MCD12Q1; Version 6) provides global land cover types at yearly intervals. Among the six different classification schemes in the MCD12Q1 data, the IGBP land cover classification (Type 1) provides 17 classes to meet the needs of the IGBP core science projects (Channan et al., 2014; Loveland & Belward, 1997). The criteria were used for dividing the classes (e.g., leaf longevity [evergreen vs. deciduous] and leaf type [broad vs. needle]). The Sturm et al. (1995, 2010) seasonal snow cover classification is defined by a unique ensemble of stratigraphic and textural characteristics of snow covers. The snow classification is primarily grouped by the effects of climate (temperature, precipitation, and wind) on the snow cover properties (e.g., snow textures, layers, and lateral variability).

The annual NASA MEaSUREs VCF product (VCF5KYR, Version 1) provides global fractional vegetation cover including three layers (percent tree cover, percent non-tree vegetation, and percent bare ground) at 0.05° spatial grid from 1982 to 2016 (Hansen & Song, 2018). In this study, the percent tree cover is used to conduct a sensitivity analysis of tree cover on the gridded SWE products. Because the fractional tree cover could have changed during the last 40 years, the annual VCF value was obtained for each gamma SWE

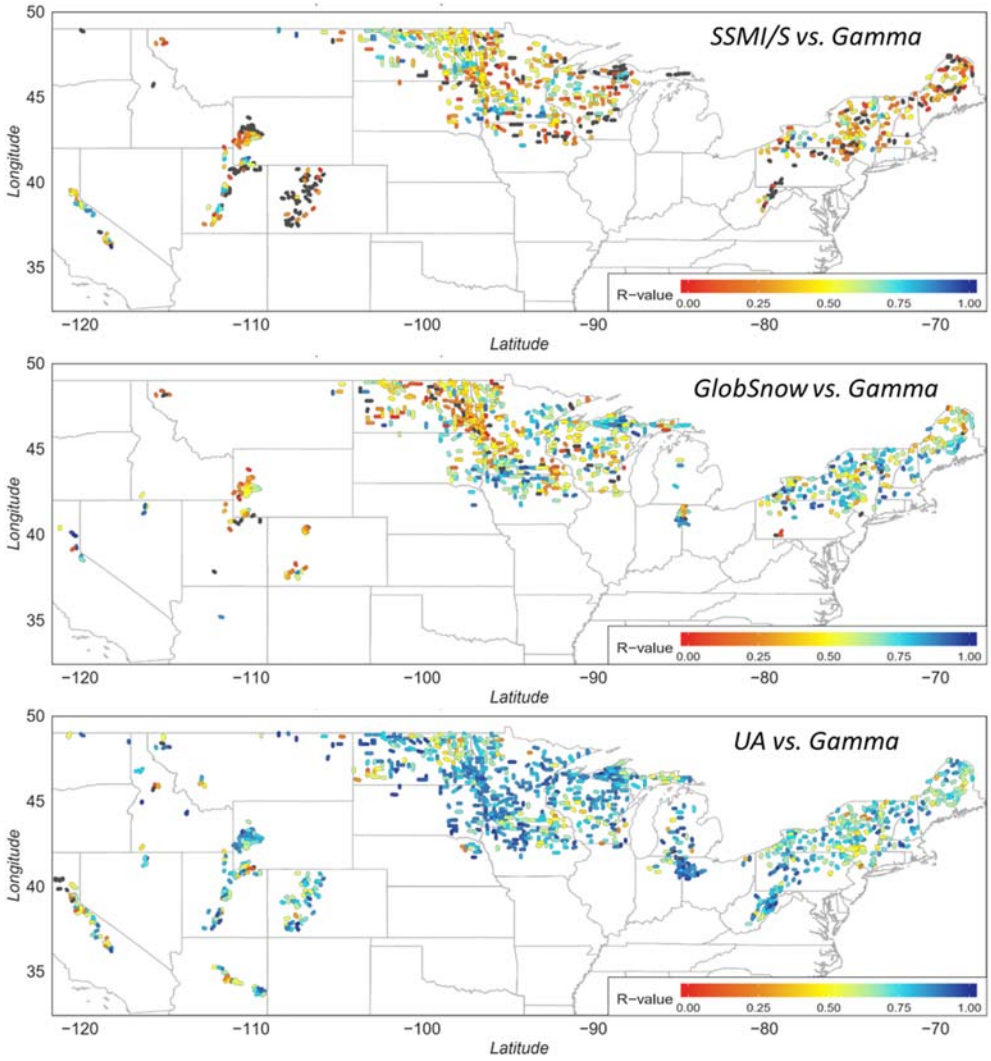

Figure 2. Correlation (*R* value) maps of daily SSMI/S, GlobSnow-2, and UA snow water equivalent with daily NOAA airborne gamma radiation snow water equivalent for each gamma flight line from 1982 to 2017 (black color represents that the *R* value is a negative value).

year. The elevation data (0.0083° grid) used in this analysis were aggregated from the Shuttle Radar Topography Mission 90-m resolution elevation data. The slope and elevation range maps (0.0083° grid; approximately 1 × 1-km grid) were obtained using the "terrain" function in the "raster" R package, which is computed using the elevation data according to Wilson et al. (2007). The elevation range value is defined as the difference between the maximum and the minimum aggregated elevation value of a cell and its eight surrounding cells. Three topographic values (slope, elevation range, and elevation) are computed for each gamma footprint by areal-weighted average.

4. Methodology

The gamma SWE observations were compared to the three gridded 4- or 25-km SWE products. The original 4-km UA SWE product was used without upscaling to 25-km grid. The gamma flight lines frequently overlapped more than one SWE pixel. The areal-weighted average SWE within the effective footprint of each gamma flight line was calculated. For each flight line, an effective polygonal measurement footprint was determined using a buffer function "gBuffer" in the "rgeos" R package around the given flight line, with a fixed diameter of 330 m (Carroll, 2001; Tuttle et al., 2018). On any day when gamma SWE measurements were collected, the gridded SWE data on the same day within the given gamma line footprint were

averaged by weighing according to the portion of the footprint contained within each SWE pixel. If the gridded SWE data were not available for a portion of the flight line footprint, the weighted SWE value was calculated using the area of the footprint with available data. However, gamma flight lines with gridded SWE data covering less than 50% of the area of flight footprint were excluded from the analysis. For further details, refer to figure 2 in Tuttle et al. (2018). The same method was applied to the tree cover fraction and three topographic characteristic data sets (slope, elevation range, and elevation). The seasonal snow cover and land cover classes for each line were selected using the "majority" function, instead of areal-weighted mean values. The classes covering more than 50% of the footprint area were used to classify the footprints in this analysis.

For evaluation, the agreements of the three gridded SWE products with airborne gamma radiation SWE were quantified by Pearson's linear correlation coefficient (R), mean absolute difference (MAD), the proportion of MAD to the mean gamma SWE ($\overline{SWE_{gam}}$), $MAD\%$, and the root-mean-square difference ($RMSD$) as follows:

$$R = \frac{cov\left(SWE_{\text{grid}}, SWE_{gam}\right)}{std\left(SWE_{\text{grid}}\right) \cdot std\left(SWE_{gam}\right)} \tag{7}$$

$$MAD = \frac{1}{n}\sum_{t=1}^{n}\left|SWE_{\text{grid},i} - SWE_{gam,i}\right| \tag{8}$$

$$MAD\% = \frac{\left(\frac{1}{n}\sum_{t=1}^{n}\left|SWE_{\text{grid},i} - SWE_{gam,i}\right|\right)}{\overline{SWE_{gam}}} \times 100 \tag{9}$$

$$\text{RMSD} = \sqrt{\frac{1}{n}\sum_{t=1}^{n}\left(SWE_{\text{grid},i} - SWE_{gam,i}\right)^2} \tag{10}$$

SWE_{grid} and SWE_{gam} refer to one of the three gridded SWE and the airborne gamma SWE values, respectively. $cov(\bullet)$ and $std(\bullet)$ refer to the covariance and standard deviation values of the given product, respectively.

5. Results

5.1. Comparison of Three SWE Products With Airborne Gamma SWE

Agreement statistics (R value and MAD, %) were calculated for each gamma flight line having six or more pairs of SWE values (Figures 2 and 3). For an example flight line, WY122, in Wyoming, the 32 pairs of historical gamma SWE and corresponding UA SWE have an R value = 0.88 (see supporting information Figure S3). SSMI/S and gamma SWE generally have a poor correlation with some regional differences (Figure 2a). In the north-central United States, the agreement is better than other regions (e.g., mean correlation and MAD of North Dakota are 0.52 and 38%, respectively). However, there are poorer agreements over northern Michigan and northeastern United States. In the western United States, the correlation is also extremely low, particularly in Colorado. The MAD spatial patterns are more readily seen (Figure 3a). MAD values exceed 75% near Lake Michigan and from Pennsylvania to Maine and are extremely high in the western United States.

The GlobSnow-2 generally agrees better with the gamma SWE than the SSMI/S result in western Minnesota, Iowa, Wisconsin, Michigan, and the northeastern United States where there are densely forested areas (Figures 2b and 3b). However, in some regions, the agreement between GlobSnow-2 SWE and gamma SWE is weaker than that of SSMI/S SWE. For example, the GlobSnow-2 SWE has lower R values (mean: 0.36) and higher MADs (mean: 43%) than SSMI/S SWE in North Dakota. While there are a limited number of comparisons in the western United States, because GlobSnow-2 SWE is masked in mountainous areas (Takala et al., 2011), there is no marked difference between GlobSnow-2 and SSMI/S.

UA SWE strongly agrees with gamma SWE across all regions (Figures 2c and 3c). In the north-central United States, there are very high correlation coefficients (mean: 0.78) with small MADs (24 mm, 31%). In the northeastern United States, UA SWE (mean R value: 0.71 and MAD: 35 mm, 44%) also has better agreement with

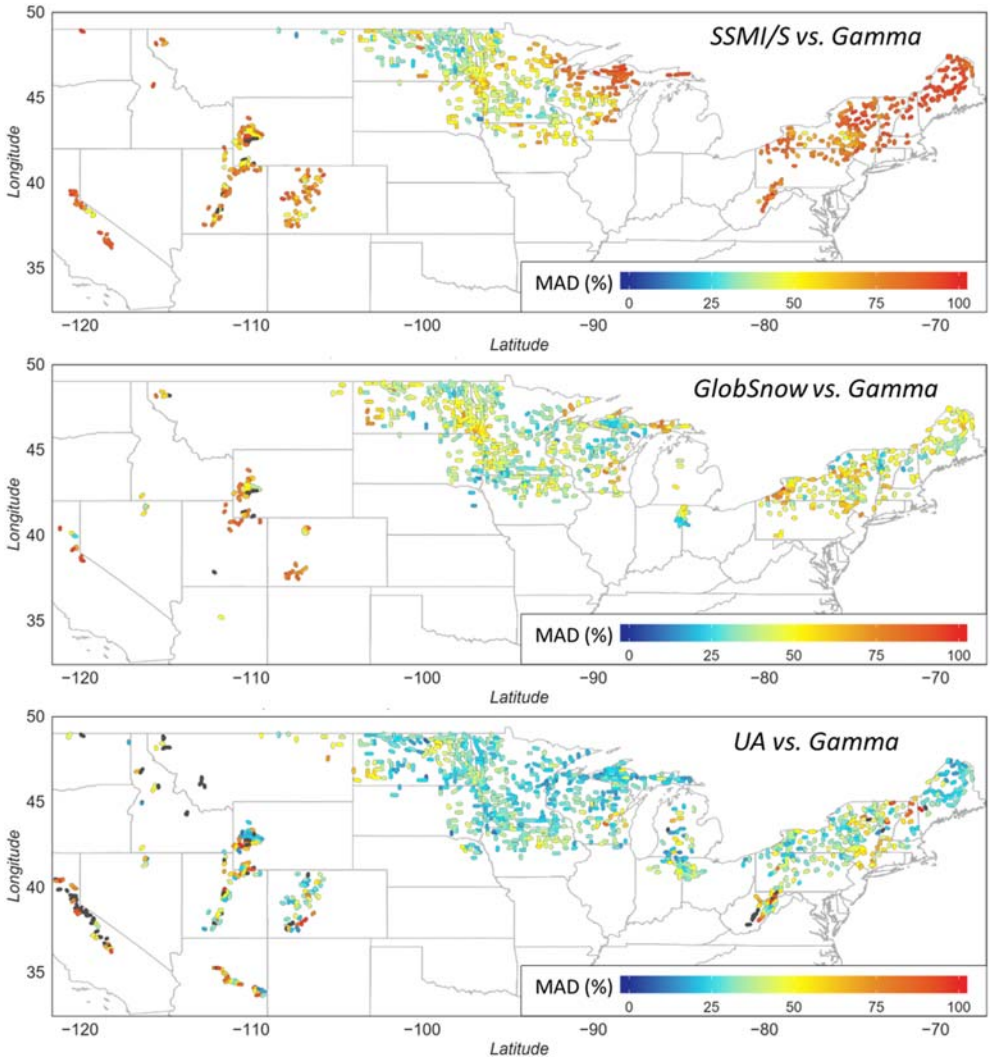

Figure 3. Mean absolute difference (MAD) maps of daily SSMI/S, GlobSnow-2, and UA snow water equivalent with daily NOAA airborne gamma radiation snow water equivalent for each gamma flight line from 1982 to 2017 (black color represents that the MAD [%] values are larger than 100%).

gamma SWE than the SSMI/S and GlobSnow-2 SWE (mean *R* value: 0.23 and 0.65 and MAD: 93 mm, 83% and 54 mm, 65%, respectively). While the two satellite-based SWE products had very poor agreement with gamma SWE in the western United States, the UA SWE agrees better, particularly in the Rocky Mountain regions including Wyoming, Arizona, Colorado, and Utah (mean *R* value: 0.07, 0.29, and 0.70 and MAD: 127, 121, and 71 mm [80%, 78%, and 59%] for SSMI/S, GlobSnow-2, and UA SWE, respectively).

5.2. Differences in SWE Agreements by Seasonal Snow Classification and Land Cover Types

The historical gamma SWE was compared to the three SWE products by the Sturm seasonal snow cover classification (Figure 4). The SSMI/S SWE extensively underestimates gamma SWE for all values of SWE. Because the SSMI/S SWE upper bound is about 172, 131, 84, 184, and 102 mm in tundra, taiga, maritime, prairie, and warm forest, respectively, none of the larger gamma values are captured. The best agreement between SSMI/S and gamma SWE is for the prairie region.

Compared to the SSMI/S SWE, GlobSnow-2 SWE has better agreement with gamma SWE, especially in the maritime, prairie, and warm forest (Table 2). Correlations of the GlobSnow-2 SWE for the three classes are 0.55, 0.35, and 0.19, which are better than those of SSMI/S SWE (0.12, 0.19, and 0.15, respectively). However, GlobSnow-2 SWE is also unable to capture high SWE values (>250 mm) in the three classes. In tundra and

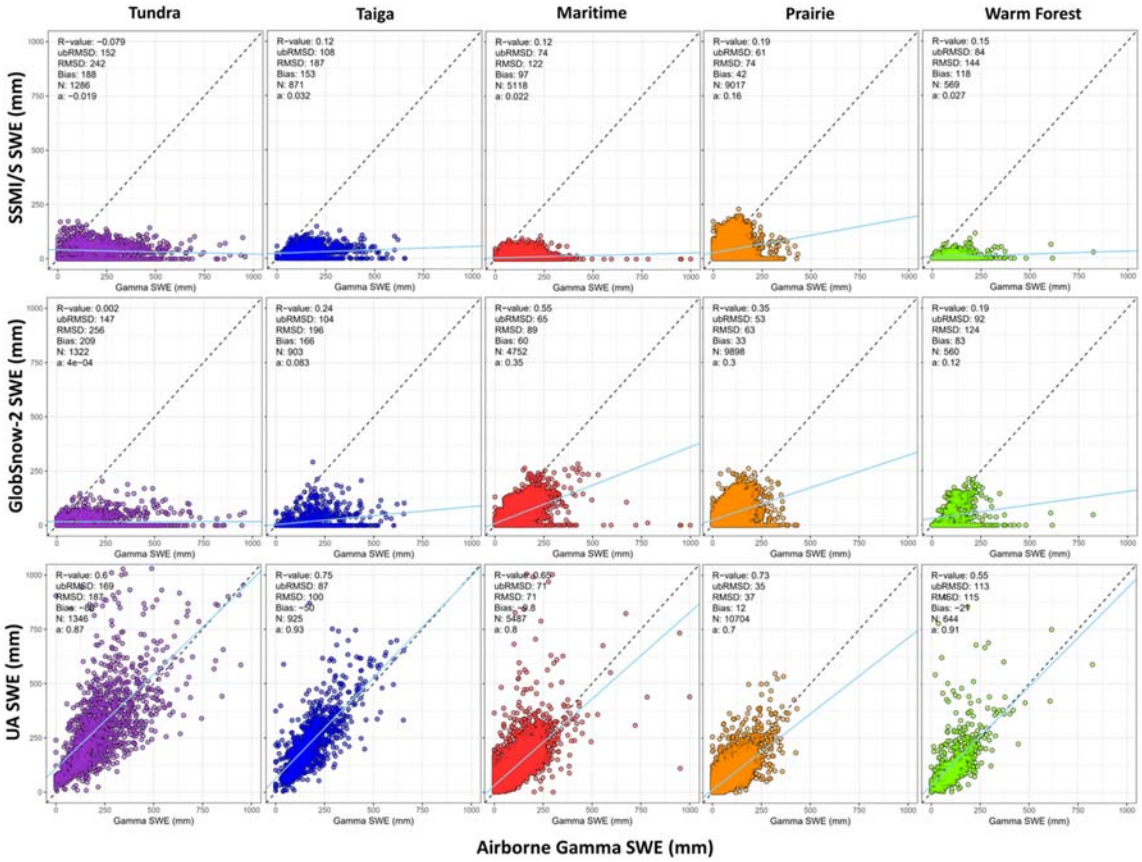

Figure 4. Comparison of daily SSMI/S (top), GlobSnow-2 (middle), and UA (bottom) snow water equivalent with daily NOAA airborne gamma radiation snow water equivalent observations from 1982 to 2017 by the Sturm et al. seasonal snow classification.

taiga, there are even larger errors (MAD: 211 and 167 mm) with gamma SWE similar to those of SSMI/S SWE (MAD: 193 and 153 mm).

UA SWE has notably stronger agreement with gamma SWE with small biases for all snow classes. The slopes are closer to 1:1 line (0.70 to 0.93), *R* values are high (0.60 to 0.75), and MAD values are moderate (119 and 73 mm) in tundra and taiga classes. The UA product tends to overestimate SWE in some cases, even though the overestimations are generally small compared to the underestimations for the other products. There are high biases in most regions with a notable number of outliers above the 1:1 line. In tundra, UA SWE has heteroscedastic errors where the differences between UA and gamma SWE gradually increase with increasing gamma SWE.

Figure 5 summarizes the spatial statistics from Figures 2 and 3 by the five seasonal snow cover classes. For SSMI/S SWE, there is a moderate overall agreement in prairie only (median *R*: 0.44 and MAD: 45%) with maritime and warm forest classes having moderate correlations but very high MAD values (85%). Tundra and taiga classes have no correlations and very high MADs. GlobSnow-2 has much better correlations and smaller MADs in the maritime and warm forest as compared to SSMI/S. However, in tundra and taiga, the GlobSnow-2 MADs are still extremely high (median: 78% and 82% for the two classes), while their correlations (median: 0.24 and 0.19) are slightly better than that of SSMI/S SWE. The UA SWE has strong correlations for all snow classes, ranging from 0.68 (median value) in tundra regions to 0.82 at the warm forest, and small MADs from 31% in tundra regions to 43% at the warm forest. As compared to SSMI/S and GlobSnow-2 products, the UA SWE and gamma SWE agreement is quite strong in tundra and taiga even though there are greater ranges of MAD values.

Because SWE products performance can be affected by land surface characteristics (e.g., vegetation types and homogeneity/heterogeneity), the above comparison was repeated based on land cover types:

Table 2
Agreement Between Daily SSMI/S, GlobSnow-2 (Glob-2), and UA SWE and Airborne Gamma SWE by the Sturm et al. Snow Cover Classification

Snow class	Gamma mean SWE (mm)	Mean (mm)			*R* value			MAD (mm)			RMSD (mm)			*N*		
		SSMI/S	Glob-2	UA	SSMI/S	Glob-2	UA	SSMI/S	Glob-2	UA	SSMI/S	Glob-2	UA	SSMI/S	Glob-2	UA
Tundra	226	37	17	307	−0.08	0.002	**0.60**	193	211	119	242	256	187	1,286	1,322	1,346
Taiga	183	29	19	233	**0.12**	**0.24**	**0.75**	153	167	73	187	196	100	871	903	925
Maritime	105	8.1	45	114	**0.12**	**0.55**	**0.65**	98	64	41	122	89	71	5,118	4,752	5,487
Prairie	81	40	47	67	**0.19**	**0.35**	**0.73**	55	44	27	74	63	37	9,017	9,898	10,704
Warm forest	128	9.1	47	147	**0.15**	**0.19**	**0.55**	118	87	58	144	124	115	569	560	644

Note. *N* is a total number of valid SWE values by the snow class; *R* values with bold indicate significance, $p < 0.05$.

evergreen needleleaf forest, deciduous broadleaf forest, mixed forest, grasslands, croplands, and cropland/natural vegetations (Figure 6; Table 3). Overall, there is similarly poor performance for the SSMI/S and GlobSnow-2 SWE products, and UA SWE has very strong agreement with gamma SWE for

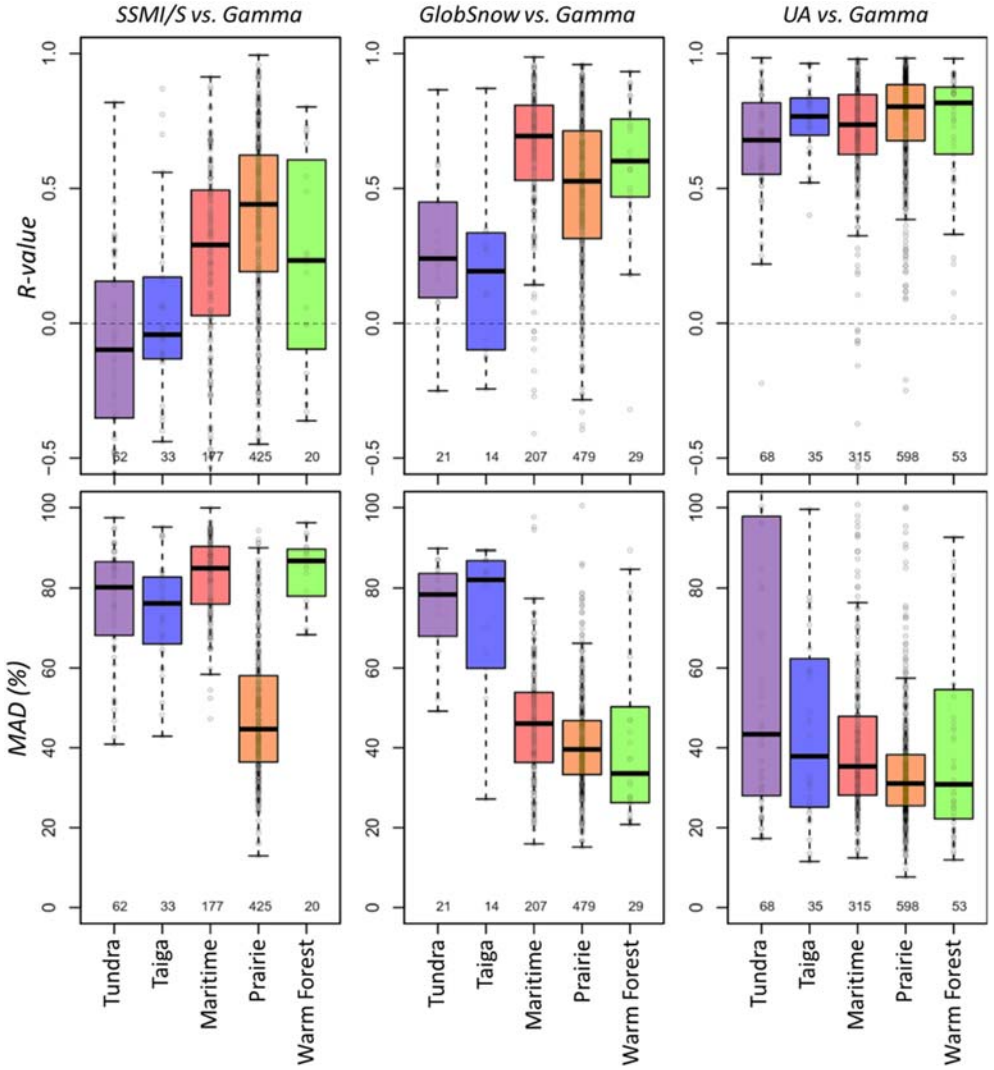

Figure 5. Box plots of correlation coefficient (*R* value) and mean absolute difference (MAD) of daily SSMI/S, GlobSnow-2, and UA snow water equivalent and daily NOAA airborne gamma radiation snow water equivalent for each gamma flight line by five snow classes (tundra, taiga, maritime, prairie, and warm forest). The number below each box plot is a total valid number of the statistic for each class.

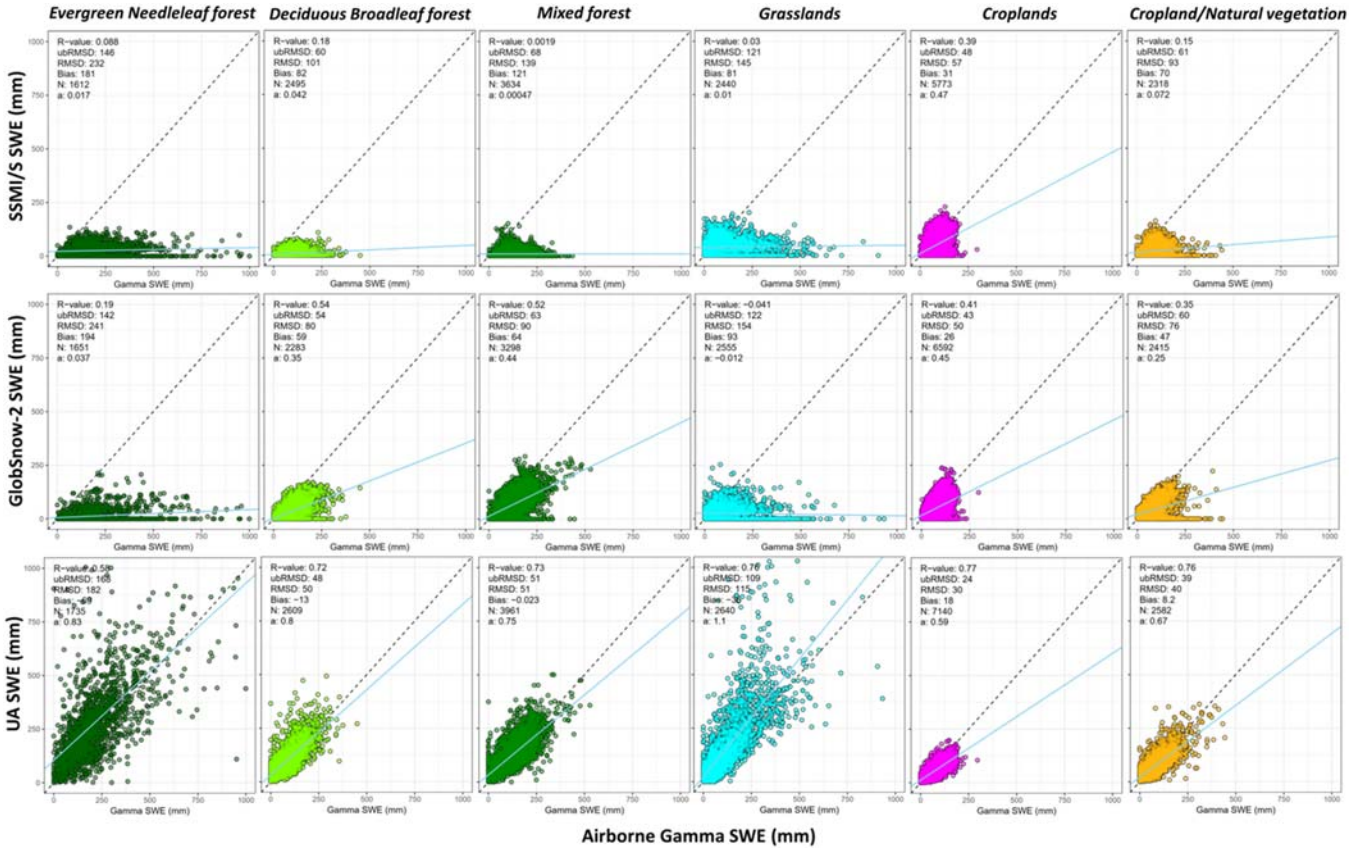

Figure 6. Comparison of daily SSMI/S (top), GlobSnow-2 (middle), and UA (bottom) snow water equivalent with daily NOAA airborne gamma radiation snow water equivalent using all available data from 1982 to 2017 by six land cover types.

all land cover types. As compared to the SSMI/S SWE, the GlobSnow-2 SWE has a better agreement with the gamma SWE in the deciduous broadleaf forest and mixed forest. However, deeper SWE values (>250 mm) were not measured by both SSMI/S and GlobSnow-2 SWE regardless of land cover types even though they are observed by the gamma SWE. In forested regions, the UA SWE has a much stronger agreement with gamma SWE as compared to SSMI/S and GlobSnow-2 SWE. To provide insights for watershed management based on the land cover within the watershed, these comparisons were repeated for the eight NOAA RFCs and are provided in Figures S1 and S2. The results indicate that the UA product provides reliable SWE values for all RFCs with the exception of the California Nevada RFC.

Figure 7 summarizes the spatial statistics from Figures 2 and 3 by land cover types. SSMI/S SWE agrees best with gamma SWE in croplands with moderate correlation (median: 0.47) and MAD values (33 mm, 42%) as compared to the other classes. Negative or very weak correlations are found in the forest classes. The GlobSnow-2 SWE has much better correlations (median: 0.70, 0.65, and 0.69) and smaller MADs (median: 47, 57, and 33 mm; 48%, 41%, and 38%, respectively) with gamma SWE for deciduous broadleaf forest, mixed forest, and cropland/natural vegetation. The differences between GlobSnow-2 and SSMI/S SWE in evergreen needleleaf forest, grasslands, and croplands are minimal. The evergreen needleleaf forest, typically located in the northern Rocky Mountain and the Sierra Nevada regions, had the weakest agreement among the six classes. The UA SWE shows very high correlations with gamma SWE for all land covers. While there are fairly large MADs in the evergreen needleleaf forest and grasslands and large interquartile ranges (median: 87 mm, 55% and 35 mm, 49%, respectively), the UA SWE MAD values are much smaller than those of the other SWE products.

In summary, SSMI/S SWE has a modest agreement only for the prairie snow class and the cropland land cover. GlobSnow-2 SWE agrees well in the maritime and warm forest snow classes and deciduous broadleaf forest, mixed forest, and cropland/natural vegetation land cover. UA SWE has strong correlations regardless

Table 3
The Same as Table 2 but by the IGBP Land Cover Types

Land cover type	Gamma mean SWE (mm)	Mean (mm)			*R* value			MAD (mm)			RMSD (mm)			*N*		
		SSMI/S	Glob-2	UA	SSMI/S	Glob-2	UA	SSMI/S	Glob-2	UA	SSMI/S	Glob-2	UA	SSMI/S	Glob-2	UA
Evergreen needleleaf forest	206	26	13	274	0.09	**0.19**	**0.58**	181	194	111	232	241	182	1,612	1,651	1,735
Deciduous broadleaf forest	92	8.5	33	104	**0.18**	**0.54**	**0.72**	82	62	36	101	80	50	2,495	2,283	2,609
Mixed forest	133	9	72	131	0	**0.52**	**0.73**	121	71	38	139	90	51	3,634	3,298	3,961
Grasslands	118	38	25	153	0.03	−0.04	**0.76**	97	102	62	145	154	115	2,440	2,555	2,640
Croplands	75	47	49	56	**0.39**	**0.41**	**0.77**	45	37	23	57	50	30	5,773	6,592	7,140
Cropland/ natural vegetation	90	20	43	81	**0.15**	**0.35**	**0.76**	72	53	29	93	76	40	1,286	1,322	1,346

Note. *N* is a total number of valid SWE values by the land cover type; *R* values with bold indicate significance, $p < 0.05$.

of class or land cover with larger MADs in tundra and taiga snow classes and the evergreen needleleaf forest and grasslands land cover. For further details about the agreements by subgroup, a series of box plots for the correlations where each of the snow (or land cover) classifications is subdivided into the six land cover types (or five snow classes) appear in Figure S4.

5.3. Effect of Tree Cover Fraction and Topographic Heterogeneity

The three historical SWE data were analyzed by tree cover fraction to determine its effect on the differences between the SWE products (Figure 8). The difference between SSMI/S and gamma SWE increases with increasing tree fraction up to 100%. The difference between GlobSnow-2 SWE and gamma SWE increased to about 70 mm (median) with increasing tree fraction up to 50%. Above 50%, the differences remain approximately constant. The differences between UA SWE and gamma SWE with forest fraction are minimal as compared to those of the other SWE products. The UA SWE slightly underestimates the gamma SWE from 0% to 80% tree fraction and then overestimates above 80%. In tree fractions below 30%, UA SWE has positive outliers (overestimation) while the SSMI/S and GlobSnow-2 SWE have negative outliers.

The impacts of three topographic characteristics (slope, elevation range, and elevation) on SWE differences were examined using the same method as the preceding tree cover analysis. Figure 9 shows that slope and elevation range (surface heterogeneity) are clearly related to the SWE difference between the three gridded products and gamma SWE. For SSMI/S SWE, slope increases from 0.7° to 1.1° show increasing differences from about 48 to 85 mm (median) and then remain constant for slopes steeper than 1.1°. The differences between GlobSnow-2 and gamma SWE are also relatively constant up to a slope of 0.7° and then increase linearly with slope. In contrast, UA SWE differences increase monotonically from −20 (at 0.1° slope) to 24 mm (at 4.0° slope) with increasing slope. The elevation range has a similar impact on the SWE differences to that of the slope. However, elevation itself does not have a coherent impact on the SWE differences. At the highest elevation (2,500 m), all SWE products have the widest interquartile range, and the UA SWE exceeds the gamma SWE.

Over 90% of the SWE values in the grasslands are found in the western United States, and all of the SWE values in evergreen needleleaf forest are in the western United States (Table S1). The SWE differences were analyzed by the topographic characteristics for these two western land cover types (Figure 10). In grasslands, the slope and elevation range (surface heterogeneity) are clearly related to the SWE difference between UA and gamma products. The SWE difference slightly increases with an increasing slope up to 3.2° and then much greater increases at higher slopes. For elevation range, there is a similar pattern where the SWE difference remains approximately constant up to 80 m of elevation range and exponentially increases by 78 mm with increasing the elevation range up to 280 m. Compared to the slope and elevation range, elevation has little effect on the SWE difference even though the interquartile range at 3,000 m elevation is very wide. There is no consistent change in the SWE differences evident with increasing either slope or elevation range

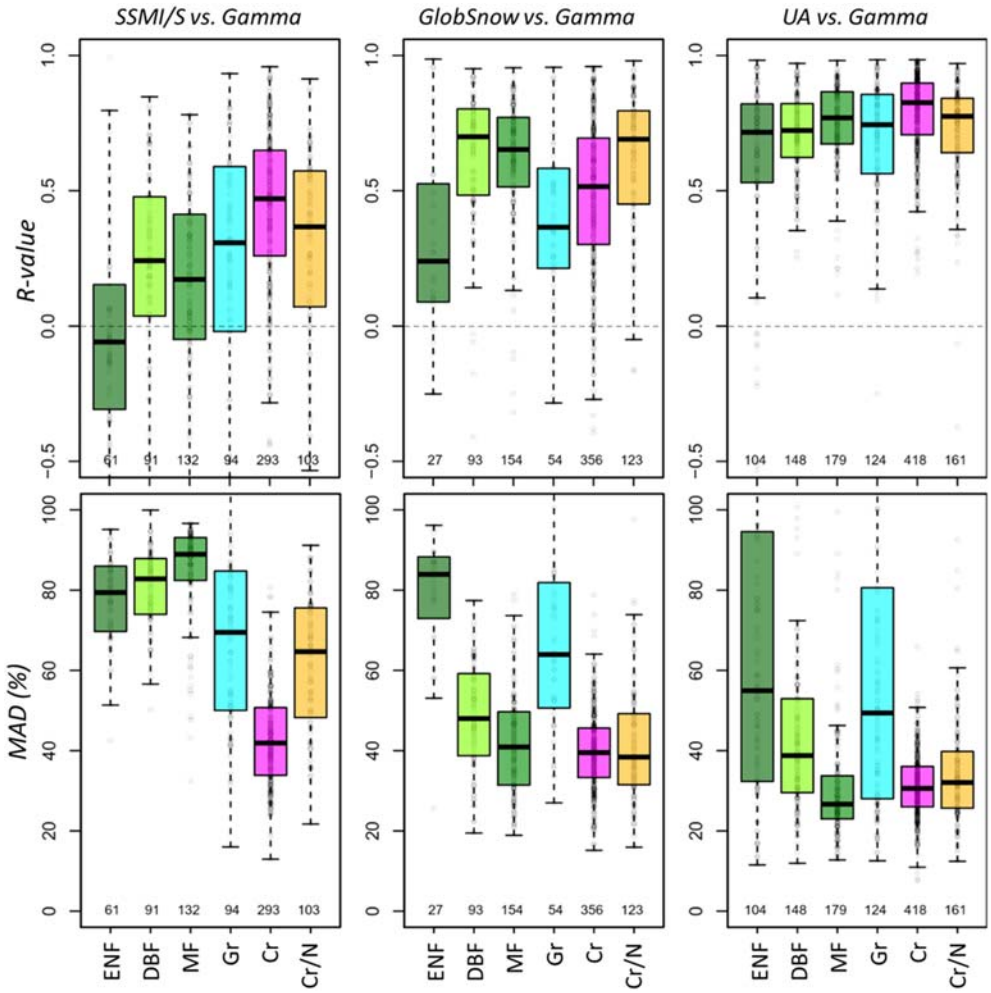

Figure 7. Box plots of correlation coefficient (*R* value) and mean absolute difference (MAD, %) of daily SSMI/S, GlobSnow-2, and UA snow water equivalent and daily NOAA airborne gamma radiation snow water equivalent for each gamma flight line by six land cover types (evergreen needleleaf forest [ENF], deciduous broadleaf forest [DBF], mixed forest [MF], croplands [Cr], cropland/natural vegetation [Cr/N], and grasslands [Gr]). The number below each box plot is a total valid number of the statistic for each class.

in evergreen needleleaf forest. The UA SWE consistently overestimates the gamma SWE for all ranges of the three topographic features.

Gamma SWE exceeds the UA SWE for tree cover fraction up to 80% but is lower than UA SWE for denser canopies (Figure 8). Over 80% of these gamma flight lines with dense canopies are in the north-central United States and northeastern United States (e.g., deciduous broadleaf forest and mixed forest; Table S2). The heavily forested areas (>80% tree cover) were further stratified by topographic characteristics for the UA and gamma SWE differences. Figure 11 shows that slope and elevation range impact the SWE difference in the heavily forested areas. The SWE difference increases by 40 and 45 mm (median) with increasing slope and elevation range up to 2.5° and 120 m, respectively. Based on the result, heterogeneous terrains, represented as slope and roughness, may partially explain the difference between UA and gamma SWE in addition to the dense tree cover.

6. Discussion

6.1. Comparison of Three SWE Products

Deep SWE was not captured by SSMI/S retrievals regardless of snow class and land cover type. This is due to a known limitation of passive microwave signal "saturation effect" for deep snowpack (approximately

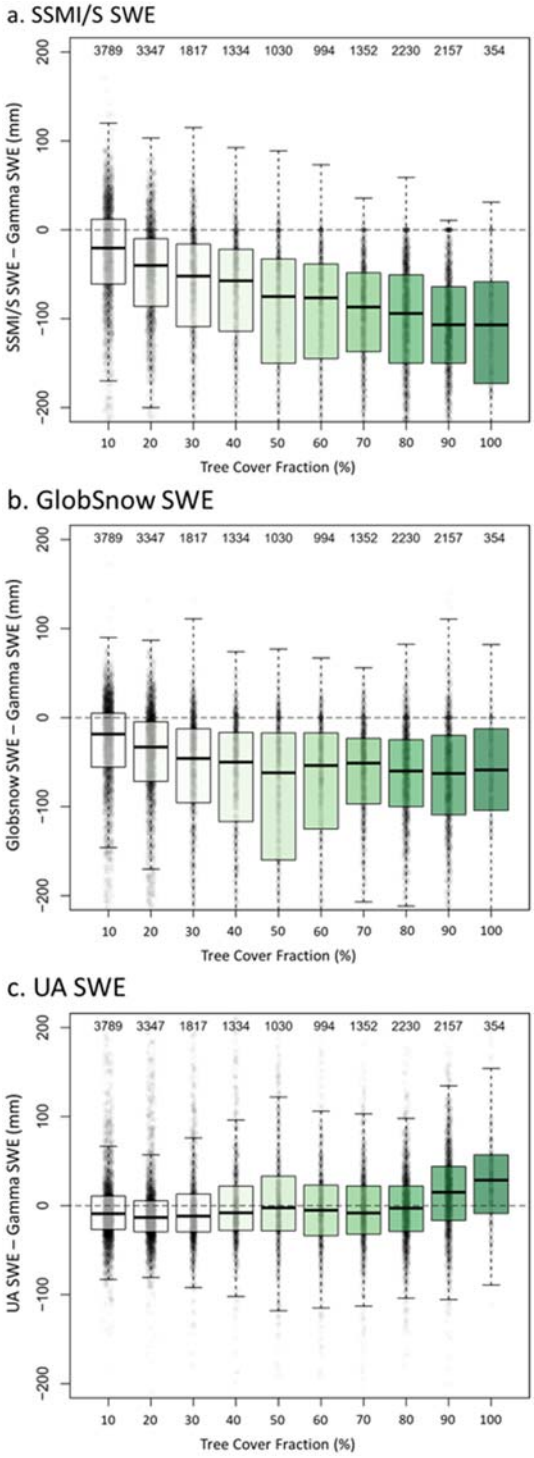

Figure 8. SWE differences of SSMI/S, GlobSnow-2, and UA products and airborne gamma radiation data by fractional tree cover (%). The white circles indicate every points in the bin.

1-m snow depth) (Dong et al., 2005; Vuyovich et al., 2014). In the deep snowpack, soil emissions are no longer detectable at the higher microwave frequency (e.g., 37 GHz). Since the GlobSnow-2 SWE product is a fusion of ground measurements of snow depth and remotely sensed data from passive microwave SSMI/S instruments, the product also appears to inherit the saturation effect (Dawson et al., 2018; Takala et al., 2011).

Both SSMI/S and GlobSnow-2 largely underestimate SWE in forested land cover types and the tundra and taiga snow classes. This may be due to the known impact of forest cover on passive microwave SWE retrievals (Foster et al., 2005; Vuyovich et al., 2014). However, similar patterns were found in grasslands, even though the average percent tree cover in grassland flight lines is typically small (mean: 9.2%). Vuyovich et al. (2014) found a disagreement between microwave and modeled SWE products in the Upper Powder Basin, Wyoming (grasslands), even though the areas have little vegetation and modest elevation ranges. This could be due to the limited availability of ground observations to inform modeled products, or it may be due to other physical effects on the microwave signal such as spatial variability and elevation gradients (Mätzler & Standley, 2000). Cai et al. (2017) mentioned that the elevation-dependent factors, besides forest fraction, affect the relationship between SWE and Tb. Another possibility is that the redistribution of SWE by wind drifting of the snowpack frequently occurs in tundra and taiga snow classes, likely resulting in larger discrepancies between the SWE products (Clow et al., 2012; Winstral et al., 2002).

The UA SWE had better performance with fewer errors in all snow and land cover classes. This may be partly because the UA SWE product (4 × 4 km) has higher spatial resolution than the SSMI/S and GlobSnow-2 SWE (25 × 25 km). However, there were fewer random errors (e.g., the degree of dispersion in Figures 4 and 5) as well as lower systematic biases (e.g., sustained overestimation/underestimation) between UA and gamma SWE. The superiority of the UA SWE data may be primarily due to the unique methodologies such as a new interpolation approach and snow density parameterization as well as the use of the reliable ground-based observations from SNOTEL SWE, COOP snow depth network, and PRISM precipitation and temperature data as inputs (Zeng et al., 2018). The UA SWE is produced by interpolating "normalized SWE" (SWE divided by accumulated snowfall), rather than SWE itself. The normalized quantities of SWE were more spatially consistent and scale-independent than original SWE quantities (Broxton, Dawson, & Zeng, 2016). A new snow density parameterization with seasonal evolutions may have contributed to the better performance compared to the other SWE products (Dawson et al., 2017). Broxton, Zeng, and Dawson (2016) mentioned that the features of snow density parameters helped overcome a common deficiency in land surface models and reanalysis products of too much ablation at near-freezing temperatures.

The gamma SWE surveys have the highest accuracy in the north-central United States (e.g., NCRFC; croplands/prairie snow class) and are extremely critical for that region because of its paucity of in situ observations (Schroeder et al., 2019; Tuttle et al., 2017). Because the spatial extent of the gamma survey is larger than most in situ observations, it also adds economic and social values in most regions that are vulnerable to spring snowmelt floods including those with established observation networks (Simonovic, 1999).

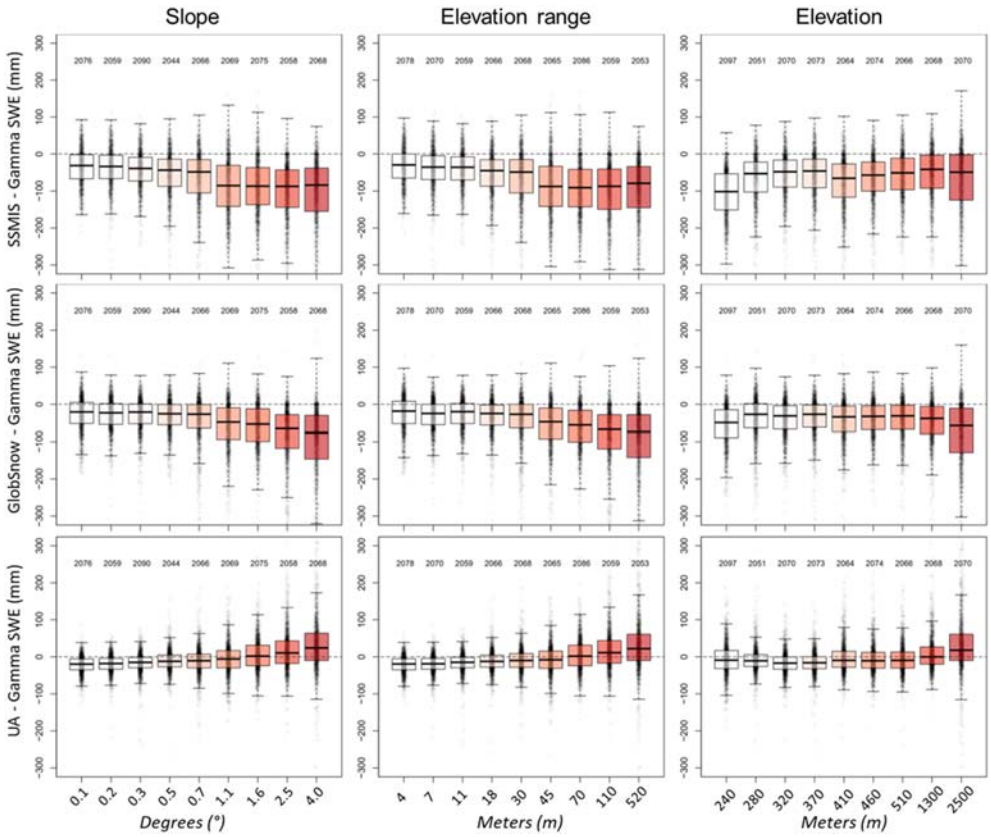

Figure 9. SWE differences of SSMI/S, GlobSnow-2, and UA products and airborne gamma radiation data by slope (degree), elevation range (m), and elevation (m). The gray circles indicate every points in the bin.

6.2. Effect of Tree Fraction

The underestimation of SSMI/S SWE is similar to the previous findings of Foster et al. (2005). In order to overcome the uncertainty, they developed a bias-corrected SWE algorithm with the forest information defined as "forest factor." For each 10th percentile of the fractional forest cover, different forest factors ranging from 1 (no forest) to 2 (100% fractional forest cover) were multiplied by the original SWE algorithm to correct the underestimation error. To test how much the uncertainty could be reduced, the corrected SSMI/S SWE was computed by considering the fractional tree cover and compared to the original SWE (Figure S5). Based on the result, the forest factor can partially reduce errors in the SSMI/S SWE. But there are still large underestimates as compared to gamma SWE, probably due to the saturation effect of passive microwave signal on the deep snowpack. GlobSnow-2 SWE performs better than SSMI/S SWE in areas with dense tree cover but not in areas with sparser tree cover. SSMI/S SWE is impacted by the attenuation of microwave signal by tree canopy cover. In contrast, the GlobSnow-2 algorithm includes ground-based snow depth measurements (Luojus et al., 2014) and forest canopy information in the HUT Snow Emission Model (Pulliainen & Hallikainen, 2001), which likely reduces errors below those expected when only the microwave emissions are considered. Regardless, GlobSnow-2 still underestimates SWE for all tree cover fractions. This could be partly related to the use of a constant low snow density (0.24 kg/m^2) to estimate GlobSnow-2 SWE without considering the seasonal evolution of snow density. The constant snow density generally represents early winter conditions (0.22, 0.26, 0.23, and 0.24 kg/m^2 in 1 October for alpine, maritime, prairie, and tundra, respectively; Sturm et al., 2010). However, approximately 85% of the gamma SWE and GlobSnow-2 SWE values are obtained in midwinter and late winter from 1 February and 30 April. There appears to be larger snow density due to compaction and snowpack metamorphism (Anderson, 2006; Dawson et al., 2017; Hill et al., 2019; Sturm et al., 2010). In this period, the typical snow densities in most snow classes from in situ measurements are larger than 0.24 kg/m^2 (e.g., maritime: 0.30–0.38 kg/m^2 and prairie: 0.24–0.32 kg/m^2; Dawson et al., 2017). Also, the underestimation of GlobSnow-2 SWE could be

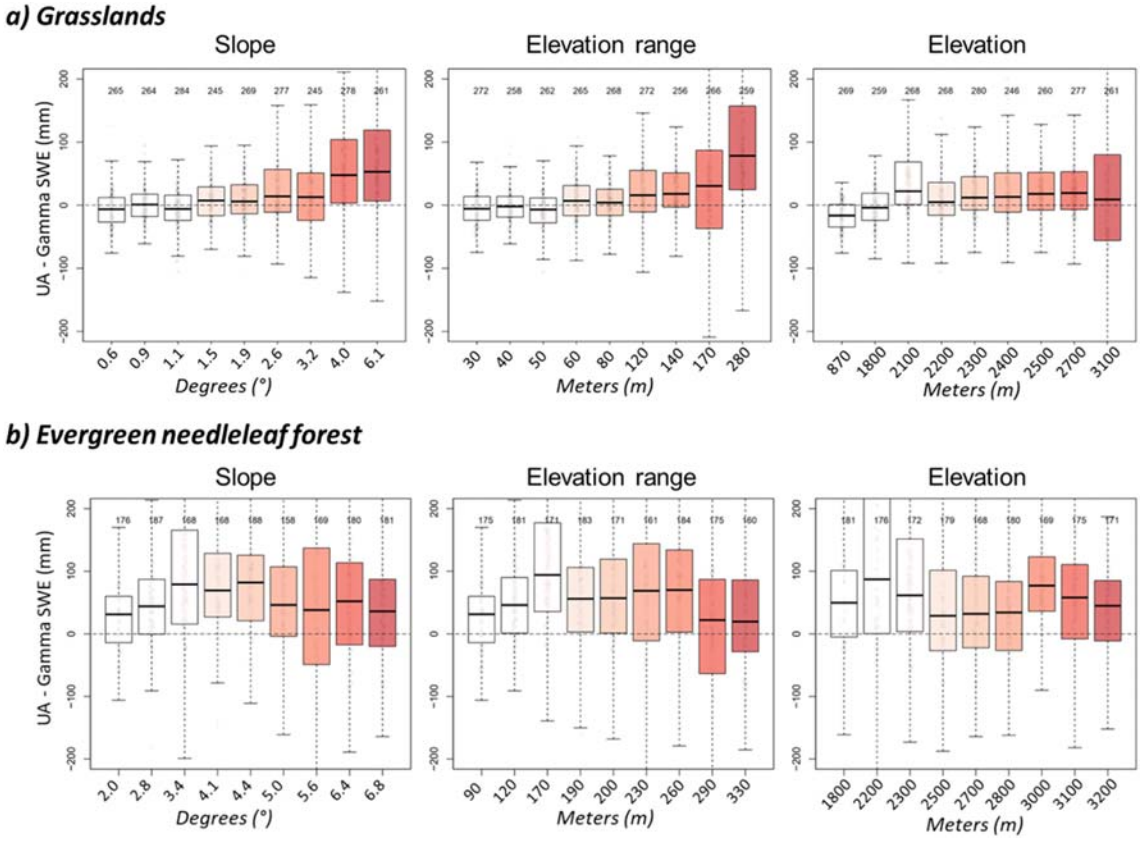

Figure 10. The same as Figure 9 but for the SWE difference between UA and gamma SWE in grassland and evergreen needleleaf forest types only.

due to the saturation effect of deep snow on the microwave signal as mentioned in the preceding section. For example, while the mean value of the deep gamma SWE (>250 mm of gamma SWE; $N = 1{,}077$) is 355 mm and UA SWE is 388 mm, the corresponding GlobSnow-2 and SSMI/S SWE was 41 and 25 mm, respectively. This indicates that the GlobSnow-2 SWE still has a similar limitation due to the saturation effect of the passive microwave signal for the deep snow (Dawson et al., 2018).

Results show that UA SWE performs well for a variety of forest covers. While the passive microwave measurements are adversely affected by forest cover, forest cover does not affect UA SWE. The superiority of the UA SWE product can be explained by the new snow density parameterization and reliable input data

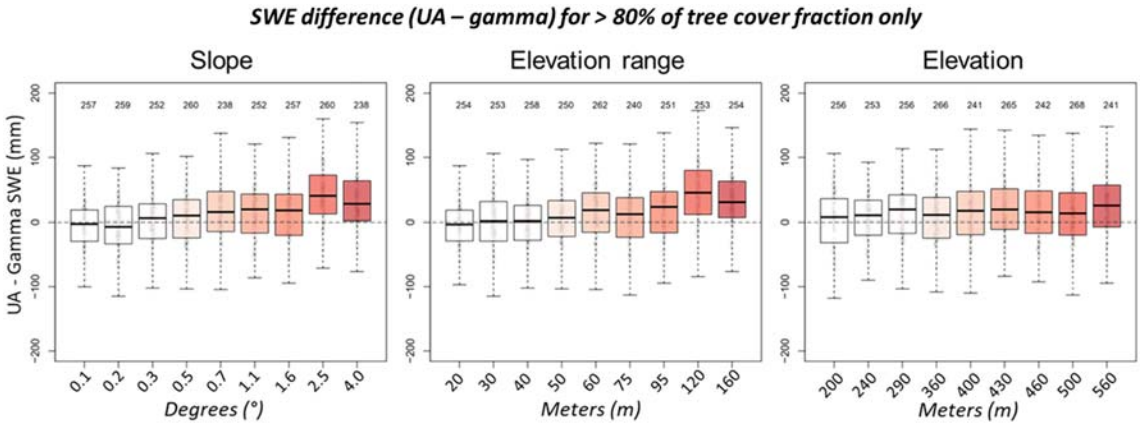

Figure 11. The same as Figure 10 but for the SWE difference between UA and gamma SWE in areas with more than 80% of tree cover fraction only.

from SNOTEL and PRISM data in forested-type regions. Unlike the other two products, the new snow density parameters used in the UA product likely reflect physical processes with an SWE evolution for all snow classes (Dawson et al., 2017). Also, the PRISM precipitation and temperature data assimilate nearly 13,000 precipitation and 10,000 temperature point stations over the conterminous United States including a few thousand stations over the northeastern United States (deciduous broadleaf forest and mixed forest types) and western United States (evergreen needleleaf forest) (Daly et al., 2008). This suggests that UA SWE may include the accuracy of PRISM precipitation data over the heavily forested regions if the partitioning of snowfall and rainfall was fairly accurate. A recent study from Dawson et al. (2018) presented that UA SWE had strong agreement with ASO SWE in California's Sierra Nevada. However, they evaluated the UA SWE using 32 ASO SWE measurements only, and the forest cover fractions in the study area were less than 35%. In addition to their results, our finding strongly supports the reliable accuracy of the UA SWE data in forested regions.

6.3. Potential Sources of Error in Gamma SWE

While the operational NOAA airborne snow survey using a gamma radiation technique has successfully provided SWE observations over the last 40 years, this method can generate errors when estimating SWE. The potential sources of error have been identified and well documented in previous studies (Carroll & Carroll, 1989a, 1989b; Glynn et al., 1988; Offenbacher & Colbeck, 1991). An uncertainty in baseline fall SM measurement can potentially introduce biases into gamma SWE estimates. The operational standard approach assumes that soil moisture conditions remain constant following the baseline fall survey. However, early-winter snowmelt and rainfall events can change the soil moisture after the fall survey, resulting in underestimation/overestimation of the gamma SWE estimates. Our recent finding in Cho et al. (2018) showed that standard gamma SWE values were improved by capturing the changes in soil moisture using daily Soil Moisture Active Passive (SMAP) satellite data. An effect of forest biomass on the accuracy of airborne SWE measurements has been explored over forested watersheds (Carroll & Carroll, 1989a; Carroll & Vose, 1984; Vogel et al., 1985). Carroll and Vose (1984) showed that there was 23 mm of RMSE between airborne gamma SWE and ground-based SWE with the moderate snowpack that ranged from 20 to 470 mm in forest environments over Lake Superior and Saint John basins. Glynn et al. (1988) found that underestimates of airborne gamma SWE (RMSE: 63 mm) could occur when gamma flight flew on forested areas with the very deep snowpack (in situ SWE: 460 mm) in the Saint John Basin over the provinces of Quebec and New Brunswick and the state of Maine.

The physical basis for a difference between UA SWE and gamma SWE in the regions with very high tree cover fractions (Figure 8) could be either an overestimation of UA SWE or an underestimation of gamma SWE or possibly both. High forest biomass may cause an underestimation of gamma SWE. Glynn et al. (1988) and Carroll and Carroll (1989a) mentioned gamma radiation emitted by the forest biomass above the snowpack as a source of error. There is a considerable amount of potassium and a minor amount of thorium in the forested-type land cover. This impact increases in a very deep snowpack because when gamma radiation coming from the ground is attenuated by the snow, the radiation emitted by the forest biomass above the deep snow can become a large portion of the radiation detected in the gamma aircraft.

Among the underestimated SWE values with the dense tree fraction, the larger underestimations occurred over flight lines with high slopes and a range of elevations within the flight footprint (Figure 9). Previous studies found that heterogeneous characteristics within a flight line, so-called uneven effect, can cause underestimates of gamma SWE (Carroll & Carroll, 1989b; Cork & Loijens, 1980). This heterogeneity is commonly caused by snow drifting or mountainous environment. A mean areal gamma SWE is calculated by integrating measures of gamma attenuation rate by an optimal counting interval during a flying (Carroll, 2001). If a large spatial variability in the snowpack exists along a flight line, the measurements of the attenuation of the gamma count rate are systematically underestimated (Cork & Loijens, 1980). For example, consider an alternating shallow and deep snowpack over a flight path. During a first counting interval, the gamma detector would measure gamma radiation from a uniform deep snowpack. Then, the flight would measure gamma radiations from snow-covered areas with different proportions of deep and shallow snowpack until the gamma detector is centered above a uniform shallow snowpack. In the transition area between deep and shallow snowpack, the larger gamma count rates tend to be measured, and the gamma rates may generate underestimates of SWE. Carroll and Carroll (1989b) found that the degree of the

underestimation is related to a variance of the distribution of ground-based SWE measurements within a flight footprint. If the variance in the gamma SWE is known, SWE underestimates can be corrected. Because our results use the standard gamma radiation SWE product without manual corrections, results could be improved by updating gamma SWE products in regions with heterogeneous characteristics. The previous studies primarily focused on the spatial variation of snowpack itself and did not consider terrain. The results in this study were not able to determine if an "uneven snow effect" was present, but terrain heterogeneity may have value as a proxy or may serve to add additional heterogeneous characteristics that also impact the gamma retrievals.

7. Conclusion and Future Perspectives

In the snow science community, observation-based long-term gridded SWE products have been developed for hydrological and climate research. However, an evaluation of the currently available SWE products has been limited due to the lack of independent SWE data sets at a continental scale. Furthermore, as land surface models and regional climate models continue to evolve at a rapid pace, independent and reliable SWE data are required to evaluate SWE outputs from the models to identify potential limitations of snow physical processes involved in each model. The historical 40-year and ongoing NOAA airborne gamma SWE record can be used as reference long-term reliable SWE across the United States and southern Canada. Even though the record has limited spatial and temporal coverages compared to the gridded satellite and reanalysis products, the record may be useful for snow hydrologists and modelers in providing accurate SWE values in various environments.

In this study, three long-term daily SWE products (more than 30 years) (SSMI/S, GlobSnow-2, and UA) were evaluated using an airborne gamma radiation SWE record collected by NOAA NOHRSC. Comparisons were made by seasonal snow cover classes and land cover types from 1982 to 2017 in the conterminous United States, and this provided several interesting insights. We found that SSMI/S and GlobSnow-2 SWE products showed similar patterns against the airborne gamma SWE: modest performances in croplands and grasslands land cover types and prairie of snow class over the north-central United States and poor performances (extremely underestimated SWE) in evergreen needleleaf forest and grasslands and tundra and taiga in mountainous regions over the western United States. These may correspond with weaknesses of inherent microwave satellite-driven signals. However, compared to SSMI/S SWE, GlobSnow-2 SWE had better agreement with gamma SWE in some forested land cover types, mixed forest, deciduous broadleaf forest, and warm forest and maritime of seasonal snow classes in the northeastern United States. UA SWE has better agreement with gamma SWE as compared to SSMI/S and GlobSnow-2 SWE in all land cover types and snow classes, while there are relatively weak agreements in the evergreen needleleaf forest and grasslands land cover and tundra snow class, which are likely due to potential limitations of UA products as well as gamma SWE in the mountainous regions (e.g., spatial heterogeneity). Through the sensitivity analysis to forest fraction, we found that UA SWE is much less affected by forest fraction, while the SSMI/S and GlobSnow-2 SWE have increasing negative biases with increasing tree fraction within the gamma flight footprint. The effect of tree cover fraction to GlobSnow-2 SWE is less than in larger fractions (>60%). With a known challenge of measuring SWE in evergreen needleleaf forest and tundra classes, unexpected weak agreement of UA SWE with gamma SWE in grasslands will be the focus of our future research to better understand the physical factors impacting on the results.

Additional use of gamma SWE products for validation of remote sensing observations and modeled SWE will likely necessitate additional inquiry into the gamma observation capabilities. Studies have shown that the improvements to the operational gamma SWE products are possible by minimizing the errors, even though potential sources of errors were identified before the 1990s (e.g., changes in fall soil moisture, the spatial variance within the footprint, and dense forest effect). Future studies can utilize state-of-the-art high-resolution earth observation products (e.g., lidar, synthetic aperture radar, and multi-spectrometer) to quantify snow or land characteristics within a gamma flight footprint to improve this valuable resource.

Acknowledgments
We would like to thank the WRR editorial team including Drs. Jessica Lundquist (editor) and Manuela Girotto (associate editor) and two anonymous reviewers for taking their time to provide constructive comments that improve this paper. The authors gratefully acknowledge support from NASA Water Resources Applied Sciences Program (NNX15AC47G). We are grateful to all who contributed to the data sets used in this study. We are grateful to the NOAA NWS NOHRSC colleagues (Tom Carroll and Carrie Olheiser) for their dedication and steady efforts to operate the airborne gamma snow survey program. The airborne gamma radiation SWE data are freely available from the NOAA NWS NOHRSC website (http://www.nohrsc.noaa.gov/snowsurvey/). The SSM/I-SSMIS brightness temperature data (Version 2) are available from the NASA National Snow and Ice Data Center (NSIDC) website (https://nsidc.org/data/NSIDC-0032). The GlobSnow-2 SWE data from 1982 to 2014 are available at http://www.globsnow.info/swe/archive_v2.0/. The UA daily 4-km SWE data (Version 1) are available from the NSIDC website (https://nsidc.org/data/nsidc-0719). The MODIS IGBP land cover classification data are downloaded from the NASA Land Processes Distributed Active Archive Center (LP DAAC) Distribution Server (https://e4ftl01.cr.usgs.gov/MOTA/MCD12Q1.006/). The annual NASA MEaSUREs Vegetation Continuous Fields (VCF) data are available from the LP DAAC Distribution Server (https://e4ftl01.cr.usgs.gov/MEASURES/VCF5KYR.001/). The slope, elevation range, and elevation raster data sets are generated by using the "terrain" function in the "raster" R-package (Version 3.0-7; https://www.rdocumentation.org/packages/raster).

References

Adams, R. M., Houston, L. L, & Weiher, R. F. (2004). The value of snow and snow information services. Report prepared for NOAA's Office of Program, Planning and Integration under contract DG1330-03-SE-1097.

Anderson, E. A. (2006). Snow accumulation and ablation model—SNOW-17. User's manual, *NOAA National Weather Service*, pp. 61. http://www.nws.noaa.gov/oh/hrl/nwsrfs/users_manual/part2/_pdf/22snow17.pdf

André, C., Ottlé, C., Royer, A., & Maignan, F. (2015). Land surface temperature retrieval over circumpolar Arctic using SSM/I-SSMIS and MODIS data. *Remote Sensing of Environment*, *162*, 1–10. https://doi.org/10.1016/j.rse.2015.01.028

Armstrong, R., Knowles, K., Brodzik, M., & Hardman, M. (1994). DMSP SSM/I-SSMIS pathfinder daily EASE-Grid brightness temperatures. Version 2. NASA National Snow Ice Data Center Distributed Active Archive Center: Boulder, CO, USA. [accessed on 1 March, 2019].

Armstrong, R. L., & Brodzik, M. J. (2001). Recent Northern Hemisphere snow extent: A comparison of data derived from visible and microwave satellite sensors. *Geophysical Research Letters*, *28*, 3673–3676. https://doi.org/10.1029/2000GL012556

Ashfaq, M., Ghosh, S., Kao, S. C., Bowling, L. C., Mote, P., Touma, D., et al. (2013). Near-term acceleration of hydroclimatic change in the western US. *Journal of Geophysical Research: Atmospheres*, *118*(19), 10–676. https://doi.org/10.1002/jgrd.50816

Barrett, A. P. (2003). *National Operational Hydrologic Remote Sensing Center Snow Data Assimilation System (SNODAS) products at NSIDC* (p. 19). Boulder, CO: National Snow and Ice Data Center, Cooperative Institute for Research in Environmental Sciences.

Brodzik, M. J. (2014). F17 vs. F13 SWE regression. Available online: http://cires1.colorado.edu/~brodzik/F13-F17swe/ [accessed on 27 March, 2019].

Broxton, P., Dawson, N., & Zeng, X. (2016). Linking snowfall and snow accumulation to generate spatial maps of SWE and snow depth. *Earth and Space Science*, *3*, 246–256. https://doi.org/10.1002/2016EA000174

Broxton, P., Zeng, X., & Dawson, N. (2016). Why do global reanalyses and land data assimilation products underestimate snow water equivalent? *Journal of Hydrometeorology*, *17*(11), 2743–2761. https://doi.org/10.1175/JHM-D-16-0056.1

Cai, S., Li, D., Durand, M., & Margulis, S. A. (2017). Examination of the impacts of vegetation on the correlation between snow water equivalent and passive microwave brightness temperature. *Remote Sensing of Environment*, *193*, 244–256. https://doi.org/10.1016/j.rse.2017.03.006

Carroll, S. S., & Carroll, T. R. (1989a). Effect of forest biomass on airborne snow water equivalent estimates obtained by measuring terrestrial gamma radiation. *Remote Sensing of Environment*, *27*(3), 313–319. https://doi.org/10.1016/0034-4257(89)90091-6

Carroll, S. S., & Carroll, T. R. (1989b). Effect of uneven snow cover on airborne snow water equivalent estimates obtained by measuring terrestrial gamma radiation. *Water Resources Research*, *25*(7), 1505–1510. https://doi.org/10.1029/WR025i007p01505

Carroll, S. S., Carroll, T. R., & Poston, R. W. (1999). Spatial modeling and prediction of snow-water equivalent using ground-based, airborne, and satellite snow data. *Journal of Geophysical Research*, *104*(D16), 19,623–19,629. https://doi.org/10.1029/1999JD900093

Carroll, T. R. (2001). Airborne Gamma Radiation Snow Survey Program: A user's guide, Version 5.0. National Operational Hydrologic Remote Sensing Center (NOHRSC), Chanhassen, 14.

Carroll, T. R., & Schaake, J. C. Jr. (1983). Airborne snow water equivalent and soil moisture measurement using natural terrestrial gamma radiation. In *In Optical Engineering for Cold Environments* (Vol. 414, pp. 208–214). Arlington, USA: International Society for Optics and Photonics. https://doi.org/10.1117/12.935888

Carroll, T. R. & Vose, G. D. (1984). Airborne snow water equivalent measurements over a forested environment using terrestrial gamma radiation. *In Proceedings of the Eastern Snow Conference*, 29, 101-115.

Chang, A. T. C., Foster, A., & Hall, D. (1987). Nimbus-7 derived global snow cover parameters. *Annals of Glaciology*, *9*, 39–44.

Channan, S., Collins, K., & Emanuel, W. R. (2014). *Global mosaics of the standard MODIS land cover type data* (p. 30). College Park, MD: University of Maryland and the Pacific Northwest National Laboratory.

Cho, E., Jacobs, J. M., Tuttle, S. E., Schroeder, R., & Olheiser, C. (2018). Improvement of airborne gamma radiation snow water equivalent measurements using SMAP soil moisture. The 75th Eastern Snow Conference (ESC), College Park, Maryland, USA, 6-8 Jun 2018.

Cho, E., Tuttle, S. E., & Jacobs, J. M. (2017). Evaluating consistency of snow water equivalent retrievals from passive microwave sensors over the north central US: SSM/I vs. SSMIS and AMSR-E vs. AMSR2. *Remote Sensing*, *9*(5), 465. https://doi.org/10.3390/rs9050465

Clow, D. W., Nanus, L., Verdin, K. L., & Schmidt, J. (2012). Evaluation of SNODAS snow depth and snow water equivalent estimates for the Colorado Rocky Mountains, USA. *Hydrological Processes*, *26*(17), 2583–2591. https://doi.org/10.1002/hyp.9385

Cooper, M. G., Nolin, A. W., & Safeeq, M. (2016). Testing the recent snow drought as an analog for climate warming sensitivity of Cascades snowpacks. *Environmental Research Letters*, *11*(8), 084009. https://doi.org/10.1088/1748-9326/11/8/084009

Cork, H. F., & Loijens, H. S. (1980). The effect of snow drifting on gamma snow survey results. *Journal of Hydrology*, *48*(1-2), 41–51. https://doi.org/10.1016/0022-1694(80)90064-5

Daly, C., Halbleib, M., Smith, J. I., Gibson, W. P., Doggett, M. K., Taylor, G. H., et al. (2008). Physiographically sensitive mapping of climatological temperature and precipitation across the conterminous United States. *International Journal of Climatology: A Journal of the Royal Meteorological Society*, *28*(15), 2031–2064. https://doi.org/10.1002/joc.1688

Dawson, N., Broxton, P., & Zeng, X. (2017). A new snow density parameterization for land data assimilation. *Journal of Hydrometeorology*, *18*(1), 197–207. https://doi.org/10.1175/JHM-D-16-0166.1

Dawson, N., Broxton, P., & Zeng, X. (2018). Evaluation of remotely-sensed snow water equivalent and snow cover extent over the contiguous United States. *Journal of Hydrometeorology*. https://doi.org/10.1175/JHM-D-18-0007.1

Derksen, C., LeDrew, E., Walker, A., & Goodison, B. (2000). Influence of sensor overpass time on passive microwave retrieval of snow cover parameters. *Remote Sensing of Environment*, *71*(3), 297–308. https://doi.org/10.1016/S0034-4257(99)00084-X

Derksen, C., & Walker, A. (2003). Identification of systematic bias in the cross-platform (SMMR and SSM/I) EASE-Grid brightness temperature time series. *IEEE Transactions on Geoscience and Remote Sensing*, *41*(4), 910–915. https://doi.org/10.1109/TGRS.2003.812003

Derksen, C., Walker, A., & Goodison, B. (2005). Evaluation of passive microwave snow water equivalent retrievals across the boreal forest/tundra transition of western Canada. *Remote Sensing of Environment*, *96*(3-4), 315–327. https://doi.org/10.1016/j.rse.2005.02.014

Dong, J., Walker, J., & Houser, P. (2005). Factors affecting remotely sensed snow water equivalent uncertainty. *Remote Sensing of Environment*, *97*, 68–82. https://doi.org/10.1016/j.rse.2005.04.010

Foster, J. L., Sun, C., Walker, J. P., Kelly, R., Chang, A., Dong, J., & Powell, H. (2005). Quantifying the uncertainty in passive microwave snow water equivalent observations. *Remote Sensing of Environment*, *2005*(94), 187–203. https://doi.org/10.1016/j.rse.2004.09.012

Georgakakos, A., Fleming, P., Dettinger, M., Peters-Lidard, C., Richmond, T. T. C., Reckhow, K., et al. (2014). Ch. 3: Water resources, *Climate Change Impacts in the United States: The Third National Climate Assessment*, edited by J. M. Melillo, T. C. Richmond and G. W. Yohe, 69-112, U.S. Global Change Research Program. https://doi.org/10.7930/J0G44N6T

Glynn, J. E., Carroll, T. R., Holman, P. B., & Grasty, R. L. (1988). An airborne gamma ray snow survey of a forested covered area with a deep snowpack. *Remote Sensing of Environment*, *26*(2), 149–160. https://doi.org/10.1016/0034-4257(88)90093-4

Goodison, B. E., Banga, A., & Halliday, R. A. (1984). Canada—United States Prairie Snow Cover Runoff Study. *Canadian Water Resources Journal*, *9*(1), 99–107. https://doi.org/10.4296/cwrj0901099

Hancock, S., Baxter, R., Evans, J., & Huntley, B. (2013). Evaluating global snow water equivalent products for testing land surface models. *Remote Sensing of Environment*, *128*, 107–117. https://doi.org/10.1016/j.rse.2012.10.004

Hansen, M. & Song, X. P. (2018). Vegetation Continuous Fields (VCF) yearly global 0.05 deg. NASA EOSDIS Land Processes DAAC. https://doi.org/10.5067/MEaSUREs/VCF/VCF5KYR.001. [accessed on 1 March, 2019].

Hill, D. F., Burakowski, E. A., Crumley, R. L., Keon, J., Hu, J. M., Arendt, A. A., et al. (2019). Converting snow depth to snow water equivalent using climatological variables. *The Cryosphere*, *13*(7), 1767–1784. https://doi.org/10.5194/tc-13-1767-2019

Kang, D.H., Barros, A.P., & Dery, S.J. (2014). Evaluating passive microwave radiometry for the dynamical transition from dry to wet snowpacks. *IEEE Transactions on Geoscience and Remote Sensing*, *52*, 3–15. https://doi.org/10.1109/TGRS.2012.2234468

Larue, F., Royer, A., De Sève, D., Langlois, A., Roy, A., & Brucker, L. (2017). Validation of GlobSnow-2 snow water equivalent over Eastern Canada. *Remote Sensing of Environment*, *194*, 264–277. https://doi.org/10.1016/j.rse.2017.03.027

Loveland, T. R., & Belward, A. S. (1997). The IGBP-DIS global 1km land cover data set, DISCover: First results. *International Journal of Remote Sensing*, *18*(15), 3289–3295. https://doi.org/10.1080/014311697217099

Luojus, K., Pullianen, J., Takala, M., Lemmetyinen, J., Kangwa, M., Eskelinen, M., et al. (2014). GlobSnow-2 final report, *Global Snow Monitoring for Climate Research, European Space Agency*. http://www.globsnow.info/docs/GlobSnow_2_Final_Report_release.pdf

Mätzler, C., & Standley, A. (2000). Relief effects for passive microwave remote sensing. *Int. J. Remote Sens.*, *21*, 2403–2412. https://doi.org/10.1080/01431160050030538

Molotch, N. P., & Bales, R. C. (2005). Scaling snow observations from the point to the grid element: Implications for observation network design. *Water Resources Research*, *41*, W11421. https://doi.org/10.1029/2005WR004229

Mote, P.W., Li, S., Lettenmaier, D.P., Xiao, M. & Engel, R. (2018). Dramatic declines in snowpack in the western US. *npj Climate and Atmospheric Science*, 1(1), 2. https://doi.org/10.1038/s41612-018-0012-1

Mudryk, L. R., Derksen, C., Kushner, P. J., & Brown, R. (2015). Characterization of Northern Hemisphere snow water equivalent datasets, 1981–2010. *Journal of Climate*. https://doi.org/10.1175/JCLI-D-15-0229.1

Offenbacher, E. L., & Colbeck, S. C. (1991). Remote sensing of snow covers using the gamma-ray technique (No. AD-A-238016/0/XAB; CRREL–91-9). *Cold Regions Research and Engineering Lab.*, Hanover, NH (United States).

Painter, T. H., Berisford, D. F., Boardman, J. W., Bormann, K. J., Deems, J. S., Gehrke, F., et al. (2016). The Airborne Snow Observatory: Fusion of scanning lidar, imaging spectrometer, and physically-based modeling for mapping snow water equivalent and snow albedo. *Remote Sensing of Environment*, *184*, 139–152. https://doi.org/10.1016/j.rse.2016.06.018

Peck, E. L., Bissell, V. C., Jones, E. B., & Burge, D. L. (1971). Evaluation of snow water equivalent by airborne measurement of passive terrestrial gamma radiation. *Water Resources Research*, *7*(5), 1151–1159. https://doi.org/10.1029/WR007i005p01151

Peck, E. L., Carroll, T. R., & VanDemark, S. C. (1980). Operational aerial snow surveying in the United States/etude de neige aérienne effectuée aux Etats Unis. *Hydrological Sciences Journal*, *25*(1), 51–62. https://doi.org/10.1080/02626668009491904

Pierce, D. W., Barnett, T. P., Hidalgo, H. G., Das, T., Bonfils, C., Santer, B. D., et al. (2008). Attribution of declining western US snowpack to human effects. *Journal of Climate*, *21*(23), 6425–6444. https://doi.org/10.1175/2008JCLI2405.1

Pulliainen, J. (2006). Mapping of snow water equivalent and snow depth in boreal and sub-arctic zones by assimilating space-borne microwave radiometer data and ground-based observations. *Remote Sensing of Environment*, *101*(2), 257–269. https://doi.org/10.1016/j.rse.2006.01.002

Pulliainen, J., & Hallikainen, M. (2001). Retrieval of regional snow water equivalent from space-borne passive microwave observations. *Remote Sensing of Environment*, *75*, 76–85. https://doi.org/10.1016/S0034-4257(00)00157-7

Royer, A., & Poirier, S. (2010). Surface temperature spatial and temporal variations in North America from homogenized satellite SMMR-SSM/I microwave measurements and reanalysis for 1979–2008. *Journal of Geophysical Research: Atmospheres*, *115*, D08110. https://doi.org/10.1029/2009JD012760

Schroeder, R., Jacobs, J. M., Cho, E., Olheiser, C. M., DeWeese, M. M., Connelly, B. A., et al. (2019). Comparison of satellite passive microwave with modeled snow water equivalent estimates in the Red River of the North Basin. *IEEE Journal of Selected Topics in Applied Earth Observations and Remote Sensing*, *12*(9), 3233–3246. https://doi.org/10.1109/JSTARS.2019.2926058

Serreze, M. C., Clark, M. P., Armstrong, R. L., McGinnis, D. A., & Pulwarty, R. S. (1999). Characteristics of the western United States snowpack from Snowpack Telemetry (SNOTEL) data. *Water Resources Research*, *35*, 2145–2160. https://doi.org/10.1029/1999WR900090

Simonovic, S. P. (1999). Decision support system for flood management in the Red River Basin. *Canadian Water Resources Journal*, *24*(3), 203–223. https://doi.org/10.4296/cwrj2403203

Stadnyk, T., Dow, K., Wazney, L., & Blais, E.-L. (2016). The 2011 flood event in the Red River Basin: Causes, assessment and damages. *Canadian Water Resources Journal*, *41*(1-2), 65–73. https://doi.org/10.1080/07011784.2015.1009949

Sturm, M., Holmgren, J., & Liston, G. E. (1995). A seasonal snow cover classification system for local to global applications. *Journal of Climate*, *8*(5), 1261-1283. https://doi.org/10.1175/1520-0442(1995)008<1261:ASSCCS>2.0.CO;2

Sturm, M., Taras, B., Liston, G. E., Derksen, C., Jonas, T., & Lea, J. (2010). Estimating snow water equivalent using snow depth data and climate classes. *Journal of Hydrometeorology*, *11*(6), 1380–1394. https://doi.org/10.1175/2010JHM1202.1

Tait, A. B. (1998). Estimation of snow water equivalent using passive microwave radiation data. *Remote Sensing of Environment*, *64*(3), 286–291. https://doi.org/10.1016/S0034-4257(98)00005-4

Takala, M., Luojus, K., Pulliainen, J., Derksen, C., Lemmetyinen, J., Kärnä, J. P., et al. (2011). Estimating Northern Hemisphere snow water equivalent for climate research through assimilation of space-borne radiometer data and ground-based measurements. *Remote Sensing of Environment*, *115*(12), 3517–3529. https://doi.org/10.1016/j.rse.2011.08.014

Tuttle, S. E., Cho, E., Restrepo, P. J., Jia, X., Vuyovich, C. M., Cosh, M. H., & Jacobs, J. M. (2017). Remote sensing of drivers of spring snowmelt flooding in the north central US. In V. Lakshmi (Ed.), *Remote Sensing of Hydrological Extremes* (pp. 21–45). Switzerland: Springer International Publishing. https://doi.org/10.1007/978-3-319-43744-6_2

Tuttle, S. E., Jacobs, J. M., Vuyovich, C. M., Olheiser, C., & Cho, E. (2018). Intercomparison of snow water equivalent observations in the Northern Great Plains. *Hydrological Processes*, *32*(6), 817–829. https://doi.org/10.1002/hyp.11459

Vogel, R. M., Carroll, T. R., & Carroll, S. S. (1985). Simulation of airborne snow water equivalent measurement errors made over a forest environment, *Proceedings of the American Society of Civil Engineers Symposium*, Denver, CO, p. 9.

Vuyovich, C. M., Jacobs, J. M., & Daly, S. F. (2014). Comparison of passive microwave and modeled estimates of total watershed SWE in the continental United States. *Water Resources Research*, *50*, 9088–9102. https://doi.org/10.1002/2013WR014734

Vuyovich, C. M., Jacobs, J. M., Hiemstra, C. A., & Deeb, E. J. (2017). Effect of spatial variability of wet snow on modeled and observed microwave emissions. *Remote Sensing of Environment*, *198*, 310–320. https://doi.org/10.1016/j.rse.2017.06.016

Walker, A. E., & Goodison, B. E. (1993). Discrimination of a wet snow cover using passive microwave satellite data. *Anuals of Glaciology*, *17*, 307–311. https://doi.org/10.3189/S026030550001301X

Wazney, L., & Clark, S. P. (2015). The 2009 flood event in the Red River Basin: Causes, assessment and damages. *Canadian Water Resources Journal*, *41*(1-2), 56–64. https://doi.org/10.1080/07011784.2015.1009949

Wilson, M. F. J., O'Connell, B., Brown, C., Guinan, J. C., & Grehan, A. J. (2007). Multiscale terrain analysis of multibeam bathymetry data for habitat mapping on the continental slope. *Marine Geodesy*, *30*, 3–35. https://doi.org/10.1080/01490410701295962

Winstral, A., Elder, K., & Davis, R. (2002). Spatial snow modeling of windredistributed snow using terrain-based parameters. *Journal of Hydrometeorology*, *3*, 524–538. https://doi.org/10.1175/1525-7541(2002)003<0524:SSMOWR>2.0.CO;2

Zeng, X., Broxton, P., & Dawson, N. (2018). Snowpack change from 1982 to 2016 over conterminous United States. *Geophysical Research Letters*, *45*, 12,940–12,947. https://doi.org/10.1029/2018GL079621